An Analytical Method to Predict the Structural Behavior of Timber-Concrete Structures With Brittle-to-Ductile Shear Connector Laws

Truong-Thanh Nguyen[a], Luca Sorelli[a,b,*], Eugen Brühwiler[b]

[a] *Department of Water and Civil Engineering, Laval University, Canada*
[b] *Structural Maintenance and Safety Laboratory (MCS), EPFL, Switzerland*

ABSTRACT

Timber-Concrete Composite (TCC) structures allow taking synergistic advantage of the properties of both materials to optimize the overall performances in terms of lightness, slenderness, acoustic insulation, vibrational behaviour and environmental footprint. In the last years, ductile shear connectors have been developed to allow the structural ductility of TCC structures. Considering the limitations of current design methods, this work aims at developing a closed-form solution for accurately predicting the nonlinear structural response of a TCC structure directly from the materials' property and the shear law of ductile connectors. In particular, we have assumed a generalized shear law based on 3 parameters which allow considering shear law from a pure elasto-plastic to pure brittle behaviour.

After a short introduction, Section 2 briefly presents the basics of the well-established elastic theory for a 2-layer composite beam with a linear shear law in terms of horizontal shear vs. slip (V_h-s) law; Section 2.3 extends the semi-analytical method proposed by Bažant and Vitek for composite structures with a generalized shear law; Sections 3 extends the previous method by developing a new closed-form analytical solution for predicting the TCC structural response for a generalized elasto-plastic V_h-s shear law described by an initial linear response up to V_{max} followed by a plastic plateau at a constant load, which can range from 0 to V_{max}; Section 4 compares the model results with the ones of existing methods and FEM analysis. Furthermore, a parametric analysis is carried out to investigate the model sensitivity to the connector parameters; Finally, Section 5 presents a simple point-by-point design procedure of which prediction accuracy of the ultimate moment, deflection and slip was statistically assessed for a large range of possible TCC structures against FEM analysis. Eventually, the effect of concrete cracking is also considered and a correction factor is proposed for engineering purpose.

1. Introduction

In the last decade, there has been a renewed interest in Timber-Concrete Composite (TCC) structures as they allow taking synergistic advantage of the lightness of timber as well as the stiffness and cost competitiveness of concrete, while enhancing vibrational behaviour, acoustic insulation, and fire resistance [1–4]. As for rehabilitation techniques, TCC technology provides cost-effective solutions for upgrading timber ceilings [5] and timber bridges as well [6]. Moreover, when compared to normal concrete floors, TCC structures can provide beneficial environmental impacts in terms of embedded energy and carbon emission [7–9].

From an historical point of view, the applications of TCC floors start mainly in the post-war reconstruction period [10]. Due to the steel high cost in the 1930s, hundreds of TCC bridges were constructed in USA

[11,12]. Today, more than 1400 TCC bridges are still in service in USA and the oldest one is about 84 years [6]. As the concrete slab protects the timber from water leaking, the TCC structural durability can be strongly enhanced.

As for the TCC structural behaviour, the slip at the material interface is practically unavoidable due to the wood deformability. The connections allow transferring the horizontal shear and engender a composite action, which strongly enhances the structural stiffness and the load-carrying capacity [13–16]. In the last decades, several connectors have been developed, such as: screws, studs [17–21], notch filled with concrete [22–26], glued notches [27], steel plates [28,29], etc. While the TCC serviceability limit states can be easily guaranteed by stiff connections, TCC structures usually show a low deformation capacity at the ultimate limit states due to the limited ductility of concrete and timber. Thus, In the late years, several ductile

* Corresponding author.
  E-mail address: luca.sorelli@gci.ulaval.ca (L. Sorelli).

Nomenclatures

A_c, A_t — cross sectional area of the concrete and timber layer, respectively [mm^2]

a_b — slope of each linear interval on V_h-s relationship of connector by Bažant's method [N/mm^2]

A_{ce}, B_{ce} — supplement parameters by CEREMA method [–]

b_c, b_t — width of the concrete and timber layer, respectively [mm]

b_b — supplement parameter of each linear interval on V_h-s relationship of connector by Bažant's method [N/mm]

$D_{e1}, D_{e2}, D_{e3}, D_{e4}$ — supplement parameters for proposed solution [–]

E_c, E_t — constant elastic modulus of concrete and timber, respectively [N/mm^2]

EA_c, EA_t — axial stiffness of concrete and timber layer, respectively [N]

EA_h — axial stiffness parameter of TCC beam [N]

EI_c, EI_t — flexural stiffness of concrete and timber layer, respectively [Nmm^2]

EI_{eff} — effective flexural stiffness of TCC beam proposed by γ-method [Nmm^2]

EI_0, EI_∞ — flexural stiffness of composite beam in No-composite and Full-composite cases, respectively [Nmm^2]

f_c^T, f_c^C — tensile and compressive strength of concrete, respectively [N/mm^2]

f_t^T, f_t^B — tensile and bending strength of timber, respectively [N/mm^2]

f_t^C — compressive strength of timber [N/mm^2]

h_c, h_t, h_i — height of the concrete, timber and interface layer, respectively [mm]

h_d — distance between the centroid of rigidity of the concrete and timber layer [mm]

I_c, I_t — inertial moment of the concrete and timber layer, respectively [mm^4]

K — elastic slip stiffness of connector by push-out test [N/mm]

k — unitary elastic slip stiffness of continuous connection system [N/mm^2]

k_s, k_u — unitary elastic slip stiffness in γ-method for SLS and ULS cases, respectively: $k_s = k$, $k_u = \frac{2}{3}k$ [N/mm^2]

L — span length of the beam (supposed working with simple supports at two ends) [mm]

l_{sp} — equidistant spacing between punctual connectors [mm]

$M_{ext}, M_{ca}, M_c, M_t$ — external moment, composite action moment, concrete moment and timber moment [Nmm]

$M_{\max}$ — maximum external moment (at mid-span) [Nmm]

M_{cr} — critical external moment (at failure of the beam) [Nmm]

N — axial force function by composite action [N]

$N_{\max}$ — maximum axial force (at mid-span) [N]

$N_{\lim}$ — asymptotic function of maximum axial force [N]

N_{cr} — critical axial force (at failure of the beam) [N]

q — function of external distributed load [N/mm]

q_0 — value of external distributed load at mid-span [N/mm]

q_D — value of q_0 at the division between elastic phase and inelastic phase [N/mm]

q_{cr} — Critical load (at failure of the beam) [N/mm]

s — slip function on interface [mm]

$s_{\max}$ — maximum slip (at the end of the beam) [mm]

$s_{\lim}$ — asymptotic function of maximum slip [mm]

s_{cr} — critical slip (at failure of the beam) [mm]

s_D — limit of slip divided elastic and inelastic behavior of connector [mm]

t — ratio of load q_0 with limit load for elastic phase q_{Da} [–]

t_{cr} — critical value of t (at failure of the beam) [–]

V_{ext} — external shear force [N]

V_H — shear force of connector by push-out test [N]

V_{H0}, V_{Hr} — Maximum shear force and residual shear force by push-out test [N]

V_h — shear flow of connector for length unit: $V_h = \frac{V_H}{l_{sp}}$ [N/mm]

V_{h0}, V_{hr} — maximum shear flow and residual shear flow for length unit [N/mm]

w — deflection function of composite beam (negative) [mm]

$w_{\max}$ — maximum deflection at mid-span (positive) [mm]

$w_{\lim}$ — asymptotic function of maximum deflection [mm]

w_{cr} — critical deflection (at the failure of the beam) [mm]

x — variable of position on the length of the beam with origin at mid-span [mm]

x_D — position function of divided point between elastic zone and plastic zone on the length of the beam [mm]

α — parameter: $\alpha = \frac{1}{d}\frac{EI_\infty}{EI_0 EA_h}$ [1/Nmm]

χ — curvature function of TCC beam [mm^{-1}]

σ_t^T, σ_t^B — tensile and bending stresses at the lower fiber of timber, respectively [N/mm^2]

φ — failure criterion of timber and beam: [–]

$\varphi_{\lim}$ — asymptotic function of failure criterion [–]

γ — parameter for evaluating composite degree of TCC beam proposed by γ-method [–]

θ — rotation function of TCC beam [–]

ω — parameter: $\omega = \sqrt{a_b d k}$ [1/mm]

---

connections, such as steel mesh plate [30], elongated composite connectors [31], screw reinforced against splitting [32], and notch connections [22,33], have been developed enhance the load-carrying capacity and ultimate deformation capacity of TCC structures [34]. Moreover, plastically designed TCC structures allow for large deformations prior to collapse and capacity of redistributing internal forces [35,36].

From a design point of view, simplified methods for TCC structures with a linear connector law were developed by Möheler and are available in design codes under the name of γ-method [37,38]. However, only semi-analytical or numerical models exist for TCC structures with connections characterized by non-linear shear behaviour [35,39,40]. In particular, Bažant and Vitek developed an iterative numerical method to analyze composite structures with connections described by a piecewise linear (or segmented) shear law, but no analytical solution was provided for the prediction of the structrual response [41]. Notably, Frangi developed a simplified design method to predict the ultimate load of TCC structures which is based on the assumption that all the connectors yield simultaneously [42]. The Frozen-

analytical model has been lately developed to predict the entire structural response of TCC beams with notch connections designed to simultaneously yield [43]. However, for general TCC structures, the connections yield gradually from the external beam ends, where the shear is maximum. Based on nonlinear analysis within Finite Element Method (FEM), Dias estimated the maximum connector spacing to allow connection to yield before the brittle failure of the timber beam [34].

This work aims at developing an accurate analytical model for predicting the full structural behaviour of ductile TCC structures by considering a simplified shear law V_h-s which is suitable for britte and ductile connectors. The following sections introduce background works and the proposed model. Then, the model validation is carried out against existing linear and numerical methods. The model sensitivity is investigated with respect to the connector parameters. An analytical design method is then proposed to predict the structural response of ductile TCC structures from three parameters describing the simplified law of a ductile connector. Finally, the design method is validated against a large variety of TCC structures and the possible effect of

concrete cracking is considered.

2. Background on analytical models for TCC structures

This section briefly recalls the main equations of existing analytical and semi-analytical models for TCC structures, especially the one of Bažant and Vitek which has been extended in this work [41]. The following hypotheses are accepted: (i) the Euler-Bernoulli beam theory is applied on each layer; (ii) concrete and timber behave linear elastically; (iii) no uplift between two layers is considered; (iv) simple supported beam with span L subjected to uniformly distributed load.

2.1. Governing equations of a composite beam

The theory of two composite beams (or layers) with a sliding interface was developed in the 1940's [44–46] and, then, successfully applied in several works for analyzing the structural behaviour of TCC structures [47–52]. Further hypotheses are considered: (i) the horizontal shear force V_h is linearly proportional to the timber-concrete interface slip; (ii) the connection system is considered as continuous and uniformly distributed. For discrete connectors, the slip modulus K and the resistance V_H are divided for the connector spacing. Based on such hypotheses, the structural behaviour of the composite beam can be described by a couple of governing differential equations as follows:

$$\begin{cases} \frac{h_d^2}{\partial x^2}\left[EI_0\frac{h_d^2 w(x)}{\partial x^2} + N(x)h_d\right] = q(x) & (a) \\ \frac{1}{k}\frac{\partial^2 N(x)}{\partial x^2} - \frac{1}{EA_h}N(x) + \frac{\partial^2 w(x)}{\partial x^2}h_d^2 = 0 & (b) \end{cases} \quad (1)$$

where

$$h_d = \frac{h_c}{2} + \frac{h_t}{2} + h_i; \quad EA_h = \frac{EA_c EA_t}{EA_t + EA_c} \quad (2)$$

$$EI_0 = EI_c + EI_t; \quad EI_\infty = EI_0 + EA_h d^2 \quad (3)$$

where $q(x)$ and $w(x)$ are respectively a function of distributed load, distributed moment and deflection of the beam. Such differential equations have been solved using classical Finite element method [39,40,53]. Note that Eq. (1a) is the Navier beam equation with the additional coupling term of $N(x)h_d$, while Eq. (1b) describes the equilibrium of the normal force on each layer. Eq. (1b) can be written as follows:

$$\frac{1}{k}\frac{\partial^2 N(x)}{\partial x^2} - \frac{EI_\infty}{EI_0 EA_h}N(x) = -\frac{h_d}{EI_0}M_{ext}(x) \quad (4)$$

Once the axial force $N(x)$ is known from Eq. (4), the threefold moment contribution can be estimated as follows:

$$M_{ca}(x) = N(x)h_d; \quad M_c = [M_{ext}(x) - M_{ca}(x)]\frac{EI_c}{EI_0};$$
$$M_t(x) = [M_{ext}(x) - M_{ca}(x)]\frac{EI_t}{EI_0} \quad (5)$$

The maximum stress at the bottom fiber of the timber section can be estimated from the timber moment M_t and the axial force N in the midspan section ($x = 0$), as follows:

$$\sigma_t^T = \frac{N(0)}{A_t}; \quad \sigma_t^B = \frac{M_t(0)}{I_t}\frac{h_t}{2} \quad (6)$$

where the subscript t stands for timber, while superscript B and T stand for Bending and Tension. It is reasonable to assume that the failure of a TCC structure occurs when the timber beam breaks in a brittle manner [1,2], i.e., with little deformation when the lower fiber of timber reaches its tensile strength by the combination of tensile and bending stresses as follows:

$$\varphi = \frac{\sigma_t^T(N)}{f_t^T} + \frac{\sigma_t^B(M_t)}{f_t^B} \leqslant 1 \quad (7)$$

Finally, the boundary conditions in terms of curvature χ, rotation θ and deflection w are as follows

$$\chi(x) = \frac{M_t(x)}{EI_t} = \frac{M_c(x)}{EI_c} = \frac{M_{ext}(x) - M_{ca}(x)}{EI_0} \quad (8)$$

$$\chi(x) = \theta'(x) = w''(x); \quad \theta(0) = 0; \quad w\left(\frac{L}{2}\right) = w\left(\frac{-L}{2}\right) = 0 \quad (9)$$

2.2. Möhler or γ-method

Equation (4) was analytically solved by assuming a linear shear-slip relationship $V_h = k \cdot s$ and a sinusoidal load $q(x) = q_0\cos(\pi x/L)$ by Möhler [54]. Such model has been adopted in the Eurocode 5 in the Annexe B for modeling TCC structures under the name of γ–method [38]. The solution in terms of axial force $N(x)$, shear flow $V_h(x)$, slip $s(x)$ and maximum deflection w_{max} reads:

$$N(x) = \frac{\gamma EA_c EA_t}{\gamma EA_c + EA_t}\frac{h_d}{EI_{eff}}M_{ext}(x); \quad V_h(x) = \frac{\gamma EA_c EA_t}{\gamma EA_c + EA_t}\frac{h_d}{EI_{eff}}V_{ext}(x) \quad (10)$$

$$s(x) = \frac{1}{k}V_h(x); \quad w_{max} = \frac{5}{384}\frac{q_0 L^4}{EI_{eff}} \quad (11)$$

where the parameters are defined as follows:

$$\gamma = \frac{1}{1 + \frac{\pi^2 EA_c}{kL^2}}; \quad a_t = \frac{\gamma EA_c}{\gamma EA_c + EA_t}h_d; \quad a_c = \frac{EA_t}{\gamma EA_c + EA_t}h_d \quad (12)$$

Finally, the effective stiffness according to the γ–method reads:

$$EI_{eff} = EI_0 + \gamma EA_c a_c^2 + EA_t a_t^2 \quad (13)$$

It is worth mentioning that the EI_{eff} was found to predict fairly well the deflection of the beam also for different load pattern [1,15]. Furthermore, for estimating the ultimate resistance, Eurocode 5 simply assumed a reduced elastic slip stiffness $k_u = 2/3\,k$ [37].

2.3. CEREMA method

In a different way from the γ–method, Renaudin analytically solved Eq. (4) by assuming a sinusoidal slip [55], which we call herein as Cerema method. Equation (4) is rewritten as follows:

$$\frac{\partial^2 N(x)}{\partial x^2} - AN(x) = -BM_{ext}(x) \quad (14)$$

where

$$A = k\frac{EI_\infty}{EA_h EI_0}; \quad B = \frac{kh_d}{EI_0} \quad (15)$$

The solution $N(x)$ is expressed as the sum of the general hyperbolic solution $N_g(x)$ as:

$$N_g(x) = \frac{C_1 + C_2}{2}e^{\sqrt{A}x} + \frac{C_1 - C_2}{2}e^{\sqrt{-A}x} = C_1\cosh(\sqrt{A}x) + C_2\sinh(\sqrt{A}x) \quad (16)$$

where constants C_1 and C_2 can be found by imposing the boundary conditions $N_{(x=-L/2)} = N_{(x=L/2)} = 0$ as follows:

$$C_1 = \frac{B}{A^2\cosh\left(\frac{L\sqrt{A}}{2}\right)}q_0; \quad C_2 = 0 \quad (17)$$

In the case of uniformly distributed load $q(x) = q_0$, the function of $N_s(x)$ reads:

$$N_s(x) = -\frac{B}{2A}q_0x^2 + \frac{B}{A}\left(\frac{L^2}{8} - \frac{1}{A}\right)q_0 \tag{18}$$

2.4. Semi-analytical solution for nonlinear V_h-s law [41]

Bažant and Vitek developed a semi-analytical method for predicting the structural response of a steel–concrete structure [41]. Such relationship was developed for stud connectors for steel–concrete composite beam for which V_h-s presents a segmented (or piecewise linear) relationship as shown in Fig. 1a, which is composed by 4 intervals: (i) perfect composite (no slip, $a_b = \infty$); (ii) hardening phase ($a_b > 0$); (iii) softening phase ($a_b < 0$); (iv) final plastic plateau ($a_b = 0$). As starting point, the equilibrium relations between axial force $N(x)$ with shear flow $V_h(x)$ and external moment $M_{ext}(x)$ with external shear force $V_{ext}(x)$ read:

$$V_h(x) = \frac{\partial N(x)}{\partial x}; \quad V_{ext}(x) = \frac{\partial M_{ext}(x)}{\partial x} \tag{19}$$

Substituting Eq. (19) into Eq. (4) yields:

$$\frac{1}{k}\frac{\partial^2 V_h(x)}{\partial x^2} - \frac{EI_\infty}{EI_0 EA_h}V_h(x) = -\frac{h_d}{EI_0}V_{ext}(x) \tag{20}$$

In the elastic phase $V_h(x) = k \cdot s(x)$ and Eq.(20) can be rewritten as follows:

$$\frac{\partial^2 s(x)}{\partial x^2} - \frac{EI_\infty}{EI_0 EA_h}ks(x) = -\frac{h_d}{EI_0}V_{ext}(x) \tag{21}$$

For each linear range of the piecewise V_h-s law shown in Fig. 1a, a linear relationship can be assumed, such as, $V_h(x) = a_b s(x) + b_b$, where a_b and b_b are constants. Thus, Eq. (21) reduces to:

$$\frac{1}{a_b}\frac{\partial^2[a_b s(x) + b_b]}{\partial x^2} - \frac{EI_\infty}{EI_0 EA_h}[a_b s(x) + b_b] = -\frac{h_d}{EI_0}V_{ext}(x) \tag{22}$$

$$\frac{\partial^2 s(x)}{\partial x^2} - \frac{EI_\infty}{EI_0 EA_h}a_b s(x) = -\frac{h_d}{EI_0}V_{ext}(x) + b_b\frac{EI_\infty}{EI_0 EA_h} \tag{23}$$

By defining the following parameters

$$\alpha = \frac{1}{h_d}\frac{EI_\infty}{EI_0 EA_h}; \quad \begin{cases} \omega = \sqrt{\alpha d a_b}, & a_b \geqslant 0 \\ \omega = \sqrt{-\alpha d a_b}, & a_b < 0 \end{cases} \tag{24}$$

the governing differential equations (22) and (23) can be recast in a more compact form as follows

$$\begin{cases} \frac{\partial^2 s(x)}{\partial x^2} - \omega^2 s(x) = -\frac{h_d}{EI_0}qx + b_b\alpha d & a_b \geqslant 0 \\ \frac{\partial^2 s(x)}{\partial x^2} + \omega^2 s(x) = -\frac{h_d}{EI_0}qx + b_b\alpha d & a_b < 0 \end{cases} \tag{25}$$

Unfortunately, the connectors work according to the different segments $V_h(x) = a_b s(x) + b_b$ in different beam segment of which positions
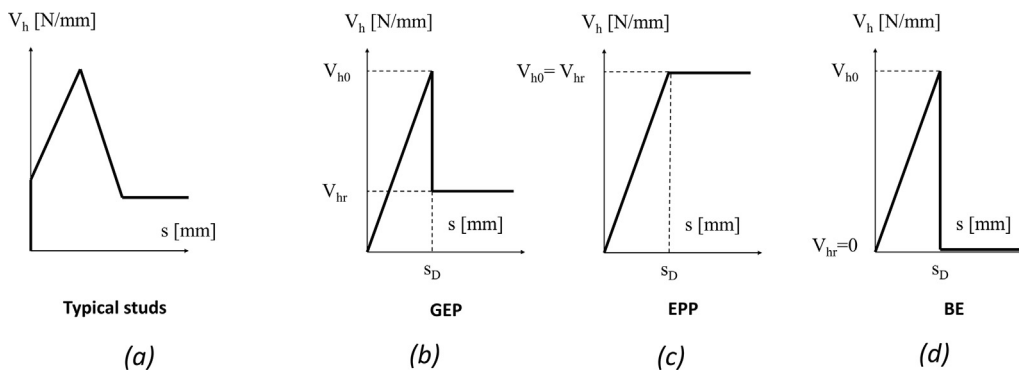
are unknown and change with the loading level. Thus, Eq. (25) can be solved only by iteration calculations in a semi-analytical manner. Interestingly, Bažant and Vitek's method reduces to CEREMA exact solution for a linear law.

3. Proposed analytical model for brittle-to-ductile shear connector laws

3.1. Shear law for connector

The scope of this section is to develop an approximate closed-form solution of the Bažant and Vitek's method by assuming a simpler law which is suitable for ductile connectors. Fig. 1b shows the simplified shear connector law assumed in this work, which comprises three possible variants of the V_h-s law, such as: (i) general elasto-plastic (GEP) where $a_b = V_{h0}/s_D = k$ and $b_b = 0$; (ii) elasto-perfectly plastic (EPP) where $a_b = 0$ and $b_b = V_{hr}$; (iii) Brittle Elastic (BE) with $V_{hr} = 0$, i.e., a sudden connector failure when the shear reaches the maximum shear flow V_{h0}. In the following section, an analytical solution of the structural response in terms of the shear connector parameters (V_{h0}, V_{hr} and s_D) is sought.

As for an example, Fig. 2a shows typical experimental shear responses of different kinds of connectors in terms of the shear V_H vs slip s. In particular, the shear law of recently developed ductile connectors is qualitatively reported, such as, steel mesh connectors [28,30], notch connectors [42,43,56], composite dowel [57], etc. In general, the higher the connector strength is, the more brittle is the structural behavior. Fig. 2b shows qualitative examples of GEP, EPP and BE shear laws V_h-s which could be used to simplify different connector shear behaviour. In particular, such approximation is more suitable for connectors with an actual ductile behaviour, at least up to a certain maximum slip. The next section will discuss further this point.

3.2. Solution in the elastic phase

For a simply supported beam with span L subjected to uniform load q_0, the external moment and external shear read as follows:

$$M_{ext}(x) = \frac{q_0 L^2}{8} - \frac{q_0 x^2}{2}; \quad V_{ext}(x) = q_0 x \tag{26}$$

At low loading level, the connectors behave elastically as described by Eq (4). The governing equation in terms of the slip and its boundary conditions reads:

$$\frac{\partial^2 s(x)}{\partial x^2} - \omega^2 s(x) = -\frac{h_d}{EI_0}q_0 x; \quad with \quad s(0) = 0; \quad \frac{\partial s}{\partial x}\left(\frac{L}{2}\right) = 0 \tag{27}$$

The exact solution of Eq. (4) is then:

$$s_{exact}(x) = (D_{e1}e^{\omega x} - D_{e1}e^{-\omega x} + D_{e2}x)q_0 \tag{28}$$

Fig. 1. (a) Connector shear law V_h-s employed by Bažant et al. [41]; Generalized connector shear laws considered in this work with (b) $V_{hr} < V_{h0}$; (c) $V_{hr} = V_{h0}$; (d) $V_{hr} = 0$.
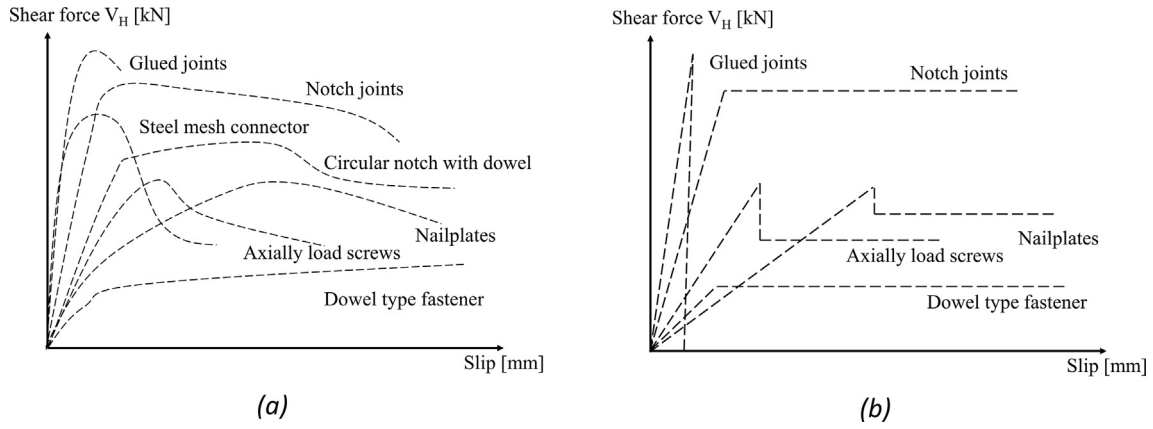
Fig. 2. (a) Examples of experimental shear law V_H-s of different connectors as measured by pushout tests [After 1]. (b) Example of simplified shear laws (GEP, EPP, BP) for different connector types.

where the following coefficients D_{e1} and D_{e2} are defined:

$$D_{e1} \stackrel{def}{=} \frac{h_d}{EI_0\omega^3\left(e^{\frac{L\omega}{2}} + e^{-\frac{L\omega}{2}}\right)}; \qquad D_{e2} \stackrel{def}{=} \frac{h_d}{EI_0\omega^2} \tag{29}$$

In the elastic phase, the slip at the beam end is proportional to the load q_0 and can be determined as follows:

$$s_{exact}\left(\frac{L}{2}, q_0\right) = \left(D_{e1}e^{\frac{L\omega}{2}} - D_{e1}e^{-\frac{L\omega}{2}} + D_{e2}\frac{L}{2}\right)q_0 = D_{e3}q_0 \tag{30}$$

where the coefficient D_{e3} is defined as follows:

$$D_{e3} \stackrel{def}{=} \left(D_{e1}e^{\frac{L\omega}{2}} - D_{e1}e^{-\frac{L\omega}{2}} + D_{e2}\frac{L}{2}\right) \tag{31}$$

As mentioned before, Eq. (28) cannot be solved analytically beyond the elastic limit due to the unknown position of the point x_D, after which the connectors undergo inelastic deformation. In this work, we employ an approximate solution based on an approximation of the exact solution Eq.(28), which respects the boundary conditions, as follows:

$$s_{appro} = \left(-\frac{4}{L^2}D_{e3}x^2 + \frac{4}{L}D_{e3}x\right)q_0 \tag{32}$$

Consequently, the other variables in the elastic phase (represented by superscript E) can be estimated as follows:

$$s_{max}^E(q_0) = s^E\left(\frac{L}{2}, q_0\right) = s_{exact}\left(\frac{L}{2}, q_0\right) = D_{e3}q_0 \tag{33}$$

$$V_h^E(x, q_0) = ks^E(x, q_0) = \frac{V_{h0}}{s_D}\left(-\frac{4}{L^2}D_{e3}x^2 + \frac{4}{L}D_{e3}x\right)q_0 \tag{34}$$

$$N^E(x, q_0) = kD_{e3}q_0\left(-\frac{4}{3L^2}x^3 + \frac{2}{L}x^2 + \frac{L}{3}\right) \tag{35}$$

$$N_{max}^E(q_0) = N^E(0, q_0) = \frac{kLD_{e3}}{3}q_0 = D_{e4}q_0 \tag{36}$$

where the coefficient D_{e4} is defined as follows:

$$D_{e4} = \frac{kLD_{e3}}{3} \tag{37}$$

The elastic deflection reduces to the following expression:

$$
\begin{aligned}
&w^E(x, q_0) \\
&= \frac{q_0}{EI_0}\left[\frac{L^2x^2}{16} - \frac{x^4}{24} - D_{e4}d\left(\frac{x^5}{5L^3} - \frac{x^4}{2L^2} + \frac{x^2}{2}\right)\right] + \frac{L^2(192dD_{e4} - 25L^2)}{1920EI_0} \\
&\quad q_0
\end{aligned} \tag{38}
$$

of which the maximum value is expressed by

$$w_{max}^E(q_0, x = 0) = -\frac{L^2(192dD_{e4} - 25L^2)}{1920EI_0}q_0 \tag{39}$$

Thus, the internal moments (M_{ca}, M_c, M_t) and the failure function (φ) can be straightforwardly calculated by Eqs. (5), (6) and (7). The elastic domain ends when the shear flow and slip at the beam ends reach the limit V_{h0} and s_D, respectively (Fig. 1b). The load at the end of the linearity q_D can be then estimated as follows

$$s_{exact}\left(\frac{L}{2}, q_D\right) = D_{e3}q_D = s_D \quad \Leftrightarrow \quad q_D = \frac{s_D}{D_{e3}} \tag{40}$$

where the letter D is employed to refer the end of linear elastic range. Consequently, the other variables at the end of the linear domain read:

$$N_{max}^D = N_{max}^E(q_D) = D_{e4}q_D = \frac{D_{e4}}{D_{e3}}s_D \tag{41}$$

$$w_{max}^D = w_{max}^E(q_D) = -\frac{L^2(192dD_{e4} - 25L^2)}{1920EI_0}q_D = -\frac{L^2(192dD_{e4} - 25L^2)}{1920EI_0}\frac{s_D}{D_{e3}} \tag{42}$$

$$\varphi^D = \varphi^E(q_D) = \frac{D_{e4}}{D_{e3}}\frac{s_D}{A_t f_t^T} + \left(\frac{s_0 L^2}{8D_{e3}} - \frac{D_{e4}}{D_{e3}}s_D d\right)\frac{E_t h_t}{2EI_0 f_t^B} \tag{43}$$

3.3. Solution in the plastic phase

When $q > q_D$, the connectors undergo to inelastic deformation. The zone of the inelastic behavior of the connections starts at the beam-ends and gradually propagates towards the mid-span. The mathematical challenge is to determinate analytically the position of point x_D, which discerns the connectors working elastically from the ones working in the inelastic range. Based on the assumption that the slip along the elastic zone has the same solution as the elastic phase, it follows

$$s^E(x_D, q_0) = s_D \quad \Leftrightarrow \quad \left(-\frac{4}{L^2}D_{e3}x_D^2 + \frac{4}{L}D_{e3}x_D\right)q_0 = s_D \tag{44}$$

Thus, x_D can be estimated from the following equation:

$$x_D(q_0) = \frac{D_{e3}q_0 - \sqrt{(D_{e3}q_0)^2 - D_{e3}q_0 s_D}}{2D_{e3}q_0}L \tag{45}$$

For the sake of simplicity, the non-dimensional load level t is defined as follows:

$$t \stackrel{def}{=} \frac{q_0}{q_D} = \frac{D_{e3}}{s_D}q_0 \quad t \geqslant 1 \tag{46}$$

Substitution of Eq. (46) into Eq. (45) yields

$$x_D(t) = \frac{L}{2}\left(1 - \sqrt{1 - \frac{1}{t}}\right) \tag{47}$$

As an example, Fig. 3(a) shows the relationship of x_D as a function of q_0 and t (q_0 and t have proportional relation according to Eq.(46)). When $t > 1$ (i.e., $q_0 > q_D$), the point x_D quickly moves forward towards the mid-span, e.g., $x_{D(t=1)} = 0.5L$ and $x_{D(t=2)} = 0.146L$. Interestingly, when $t > 2$, x_D moves more slowly to the asymptotic value ($x = 0$). Fig. 3(b) shows the distribution of shear flow V_h along the beam length. In the interval $[-x_D, x_D]$, the connector system presents elastic behavior, which is called the elastic zone. At the point x_D (and $-x_D$), the shear flow is the maximum value V_{h0}. Beyond x_D to the end of each side (left and right), the connectors undergo plastic deformation and shear flow stays at constant value V_{hr}. In the following, we will call the left and right plastic zone *P1* and *P2*, respectively.

The shear flow can be then described as follows

$$V_h^P(x, t) = \begin{cases} V_h^E(x, q_D) & x \le x_D(t) x \le x_D(t) \\ V_{hr} & x \ge x_D(t) \end{cases} \tag{48}$$

where superscript *P* stands for Plastic phase. In the right plastic zone *P2*, the governing equation in Eq. (25) becomes

$$\frac{\partial^2 s^{P2}(x, t)}{\partial x^2} = -\frac{h_d}{EI_0}\frac{t s_D}{D_{e3}}x + \alpha h_d V_{hr} \tag{49}$$

with the following boundary conditions:

$$s^{P2}(x_D, t) = s_D; \quad \frac{\partial}{\partial x}s^{P2}\left(\frac{L}{2}, t\right) = 0 \tag{50}$$

The distribution of slip function in the plastic phase is now recast as follows:

$$s^P(x, t) = \begin{cases} s^E(x, q_D) & x \le x_D \\ s^{P2}(x, t) & x \ge x_D \end{cases} \tag{51}$$

Thus, the maximum slip at the beam end reads:

$$s_{max}^P(t) = s^{P2}\left(\frac{L}{2}, t\right)$$
$$= s_D + \frac{1}{48 D_{e3}EI_0}h_d L^3 s_D(t-1)\left(3 - \sqrt{1 - \frac{1}{t}}\right) - \frac{1}{8}\alpha V_{hr}h_d$$
$$L^2\left(1 - \frac{1}{t}\right) \tag{52}$$

The axial force is estimated by integration of the shear flow along the plastic zone as follows

$$N^{P2}(x, t) = V_{hr}\left(\frac{L}{2} - x\right) \tag{53}$$

Analogously, in the elastic zone limited condition at x_D, N can be estimated:

$$N^{P1}(x_D, t) = N^{P2}(x_D, t) \tag{54}$$

The maximum axial force at mid-span section ($x = 0$) is then a function of t:

$$N_{max}^P(t) = N^{P1}(0, t)$$
$$= \frac{1}{2D_{e3}}\left\{[V_{hr}LD_{e3} - s_D D_{e4}(2t+1)]\sqrt{1 - \frac{1}{t}} + 2D_{e4}s_D t\right\} \tag{55}$$

The maximum moment at mid-span section ($x = 0$) is calculated as a function of *t*:

$$M_{max}(t) = \frac{L^2}{8}q_0 = \frac{L^2}{8}\frac{s_D}{D_{e3}}t \tag{56}$$

The maximum deflection at mid-span section ($x = 0$) is calculated as a function of *t*:

$$w_{max}(t)$$
$$= \frac{2\sqrt{t(t-1)}}{375t^2(2t^2 - t - 1)D_{e3}EI_0}$$
$$\begin{Bmatrix} \frac{625}{256}(2t+1)t^2\sqrt{t(t-1)}s_D L^4 \\ -\frac{125}{8}(t-1)\left(t^2 + t + \frac{1}{4}\right)V_{hr}dD_{e3}L^3 \\ -\frac{75}{2}\left[\left(t + \frac{1}{2}\right)t^2\sqrt{t(t-1)} - \left(t + \frac{1}{2}\right)(t-1)\left(t^2 + \frac{1}{2}t\right. \\ \left. + \frac{3}{8}\right)\right]M \end{Bmatrix}$$

where $M = D_{e4}ds_D L^2 - \frac{75}{2}\left[\left(t + \frac{1}{2}\right)t^2\sqrt{t(t-1)}\right.$

$$\left. -\left(t + \frac{1}{2}\right)(t-1)\left(t^2 + \frac{1}{2}t + \frac{3}{8}\right)\right]D_{e4}ds_D L^2 \tag{57}$$

Finally, the failure function can be simplified as follows:

$$\varphi^P(t) = \frac{N_{max}^P(t)}{A_t f_t^T} + [M_{max}(t) - N_{max}^P(t)d]\frac{E_t h_t}{2EI_0 f_t^B} \tag{58}$$

Lastly, the deformation variables (deflection, curvature and rotation) can be estimated by imposing the symmetry conditions as follows

$$w^{P1}(x_D, t) = w^{P2}(x_D, t); \quad w^{P2}\left(\frac{L}{2}, t\right) = 0;$$
$$\theta^{P1}(x_D, t) = \theta^{P2}(x_D, t); \quad \theta^{P1}(0, t) = 0; \quad \chi^{P1}(x_D, t) = \chi^{P2}(x_D, t); \tag{59}$$

3.4. Asymptotic limits

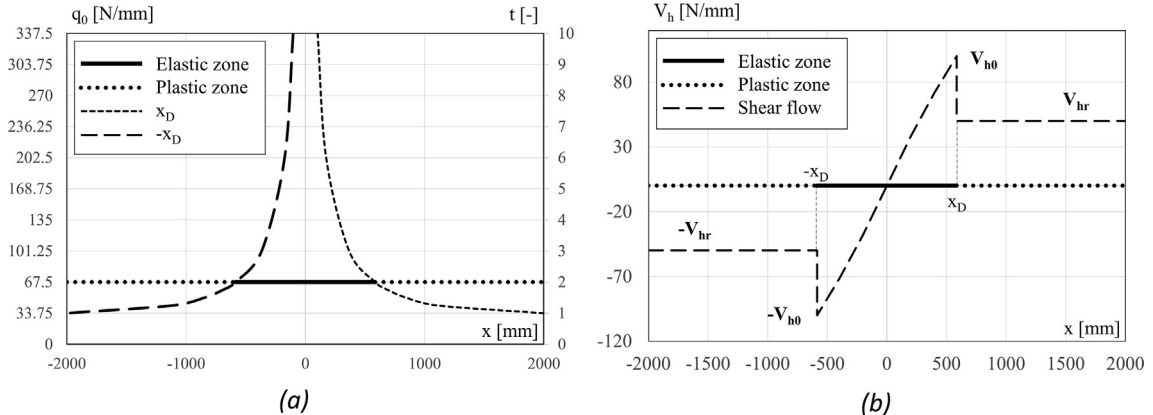Interestingly, when the non-dimensional load t (or q_0) increases

Fig. 3. (a) Division point x_D as a function of load; (b) Shear flow as a function of x.

during the plastic phase, the function N tends to become linear for high values of t. That is, once that all the connectors have gradually plasticized, the structural behaviour becomes again linear. In more details, N tends to an asymptotic limit as follows:

$$
\begin{aligned}
N_{\lim} &= \lim_{t \to \infty} N_{\max}^P(t) \\
&= \lim_{t \to \infty} \left\{ \frac{1}{2D_{e3}} \left[(V_{hr} L D_{e3} - s_0 D_{e4}(2t+1)) \sqrt{1 - \frac{1}{t}} + 2D_{e4} s_0 t \right] \right\} \\
&= \frac{V_{hr} L}{2}
\end{aligned}
\tag{60}
$$

Similarly, the asymptotic limits for slip, failure function and deflection of structure as follows:

$$
\begin{aligned}
\varphi_{\lim} &= \lim_{t \to \infty} \varphi^P(t) = \frac{L^2 E_t h_t}{16 EI_0 f_t^T} q_D t - \frac{L(EA_t h_d h_t f_t^T - 2EI_0 f_t^B)}{4A_t EI_0 f_t^T f_t^B} V_{hr} \\
&= \frac{L^2 E_t h_t}{16 EI_0 f_t^T} q_0 - \frac{L(EA_t h_d h_t f_t^T - 2EI_0 f_t^B)}{4A_t EI_0 f_t^T f_t^B} V_{hr}
\end{aligned}
\tag{61}
$$

$$
\begin{aligned}
s_{\lim} &= \lim_{t \to \infty} s_{\max}^P(t) = s_D + \frac{h_d L^3 s_D (t - 0.75)}{24 D_{e3} EI_0} - \frac{1}{8} \alpha h_d L^2 V_{hr} \\
&= s_D + \frac{h_d L^3}{24 EI_0} \left(q_0 - 0.75 \frac{s_D}{D_{e3}} \right) - \frac{1}{8} \alpha h_d L^2 V_{hr}
\end{aligned}
\tag{62}
$$

$$
\begin{aligned}
w_{\lim} &= \lim_{t \to \infty} w_{\max}^P(t) = \frac{5L^4}{384 EI_0} \frac{s_D}{D_{e3}} t - \frac{L^3 h_d}{24 EI_0} V_{hr} \\
&= \frac{5L^4}{384 EI_0} q_0 - \frac{L^3 h_d}{24 EI_0} V_{hr}
\end{aligned}
\tag{63}
$$

Fig. 4 compares the asymptotic limits (dashed lines) with the full functions (bold lines) for different residual shear strength ($V_{hr} = 0\%$, 50% and 100% V_{h0}). Clearly, all the main variables describing the TCC structural behaviour tends to linear asymptotic limits. It is worth noticing that such asymptotic functions are composed by two parts: (i) one part depending on the load q_0, which corresponds to the case of no-

composite action; (ii) the second part depending on the residual strength $V_{hr}(0)$.

4. Results and discussion

In the following, as for validation, the results of the proposed model have been compared against: (i) a numerical FEM models which has been well validated against several experimental tests on TCC beams [13,57,58]; (ii) analytical models which are commonly used of which applicability is limited by the assumed linearity of the connection shear law [54]; (iii) a push-out model which has been validated for ductile connectors in a previous work [35,59].

4.1. Validation of the proposed model against existing elastic methods and FEM analysis

First, the developed method was compared against analytical methods (γ-method and CEREMA method) and a non-linear FEM model [39]. Fig. 5a shows a case study of TCC beam for a bridge application, which is chosen from the work of Gendron et al. [58]. As for the connection law, we arbitrarily consider an EP law (Fig. 1b) with $V_{h0} = 100$ N/mm, $s_D = 1$ mm, $V_{hr} = 50$ N/mm, $k = 100$ N/mm^2. Thus the model parameters presented can be estimated as follows: $d = 250$ mm, $EA_c = 1.50 \times 10^9$ N, $EA_t = 6.00 \times 10^8$ N, $EA_h = 4.29 \times 10^8$ N, $EI_c = 1.25 \times 10^{12}$ Nmm^2, $EI_t = 8.00 \times 10^{12}$ Nmm^2, $EI_0 = 9.25 \times 10^{12}$ Nmm^2, $EI_\infty = 3.60 \times 10^{13}$ Nmm^2, $D_{e1} = -4.53 \times 10^{-3}$, $D_{e2} = 2.97 \times 10^{-5}$, $D_{e3} = 2.96 \times 10^{-2}$, $D_{e4} = 3.95 \times 10^3$, $\alpha = 3.636 \times 10^{-11}$, $\omega = 9.534 \times 10^{-4}$, $q_D = 33.73$ N/mm.

4.1.1. Validation in the elastic domain

Fig. 6 compares the solution of the proposed method against linear methods (γ–method and CEREMA method) in terms of slip s, axial force
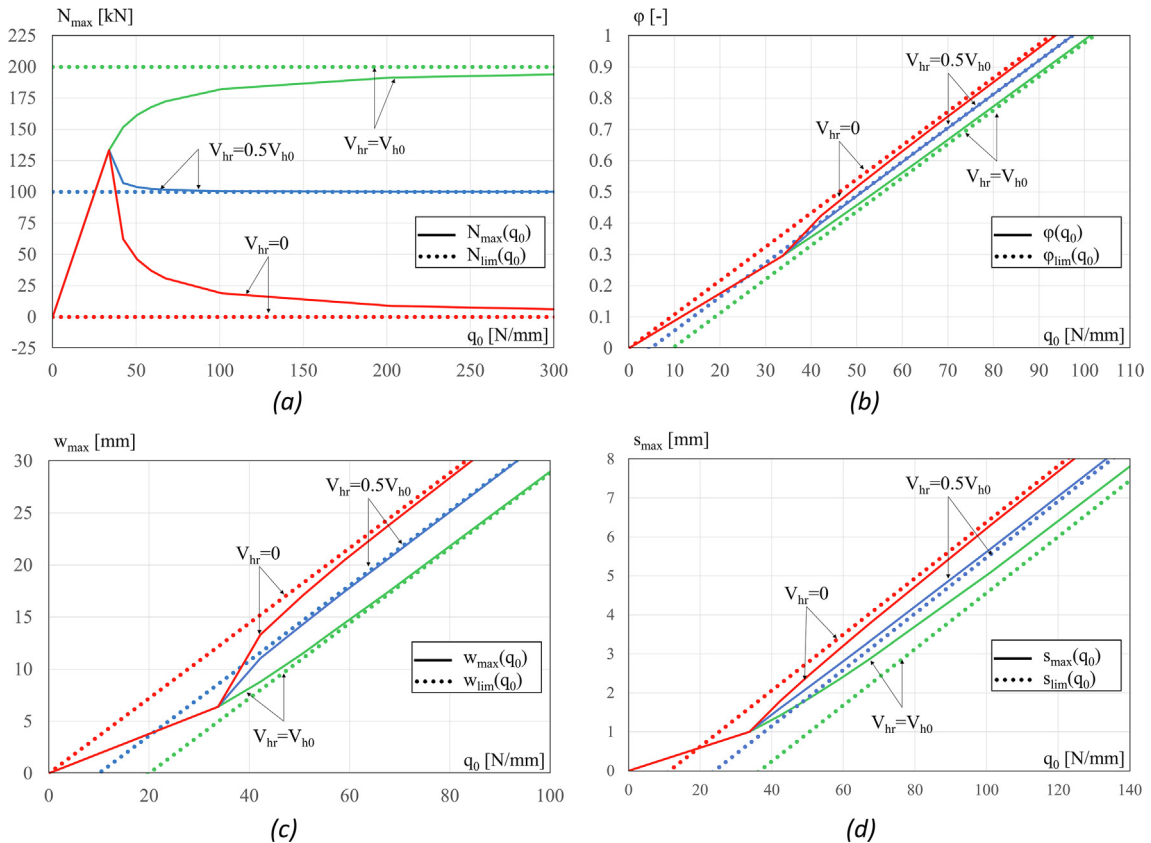

Fig. 4. Asymptotic limits for (a): Failure function vs. load; (b): Maximum slip vs. load; (c): Maximum axial force vs. load; (d): Maximum deflection vs. load.
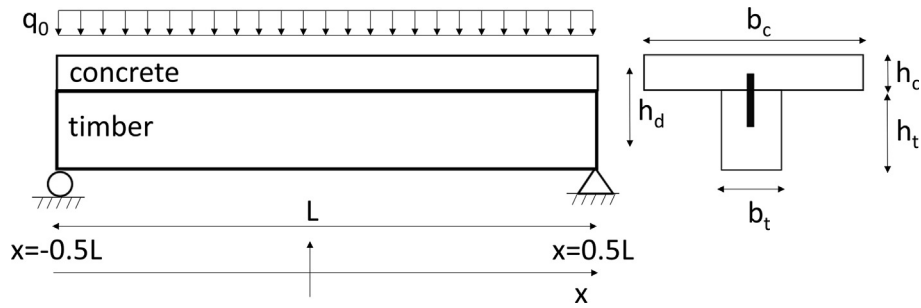
Fig. 5. Case study of TCC structure for comparing the different methods.

N, timber moment M_t and deflection w in the elastic range at the load level of $t = 3\%$ (i.e., $q = 1$ N/mm and $q_D = 33.73$ N/mm). The results of γ–method are identical with the exact solution (which is CEREMA in this case), while the proposed solution shows very close results with a maximum discrepancy of 5% greater. In particular, the proposed approximate solution is slightly stiffer in terms of deflection and the slip prediction, while it slightly overestimates the axial force and timber moment.

4.1.2. Validation in the plastic domain

As for the plastic domain, Fig. 7 compares the solution of the proposed method against linear methods (γ–method with $k_u = 2/3\,k$ and CEREMA method) and a nonlinear FEM model for TCC structures [60] at a load level of $t = 1.48\%$ (i.e., $q = 50$ N/mm greater of q_D). The considered FEM model, which allows considering any kind of non-linear V_h-s law and concrete cracking, has been well validated again several experimental results of TCC beams [60]. In this context, the FEM solution is considered as the exact or reference solution. The proposed solution predicts with high accuracy the exact solution in terms of the axial force N and timber moment M_t, while linear solutions (CEREMA method and γ–method with k_u at ULS) strongly overestimate N and underestimate M_t. As for the slip function (Fig. 7a), the proposed solution slightly underestimates the exact solution by predicting a longer elastic zone. In the same way, Fig. 7d shows that the plastic plateau of the proposed solution is slightly smaller than the exact solution. Yet, the linear methods show much less accurate results in predicting the distribution of the slip s and shear flow V_h.

Table 1 compares the considered methods in terms of the prediction of main variables at the end of the elastic domain ($q_0 = q_D$) and at structural failure $\varphi = 1$ based on Eq. (7). The percentage error with respect to the exact FEM solution is also reported between quotes. For the sake of comparison, the analytical solutions for no and full composite action are also reported. The capacity of the proposed approximate method is satisfactory in predicting the load at the end of linearity and at failure. The proposed method slightly overestimates the deflection at the end of linearity of about (-5.3%), but it predicts well the deflection at ultimate limit state (+0.3%)

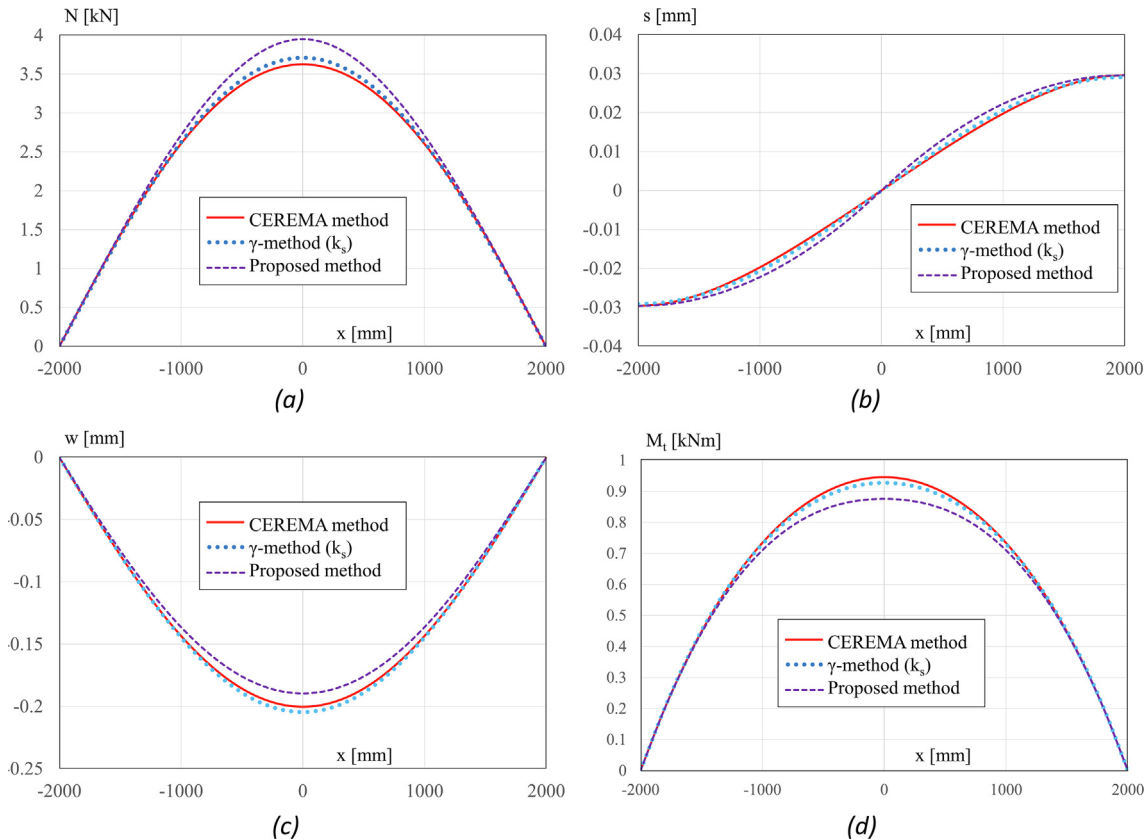Finally, Fig. 8 compares the proposed method and its asymptotic

Fig. 6. Comparison of different methods in the elastic domain at t = q/q_D = 3% in terms of distribution of (a) slip s; (b) axial force N; (c) timber moment M_t and (d) deflection w.
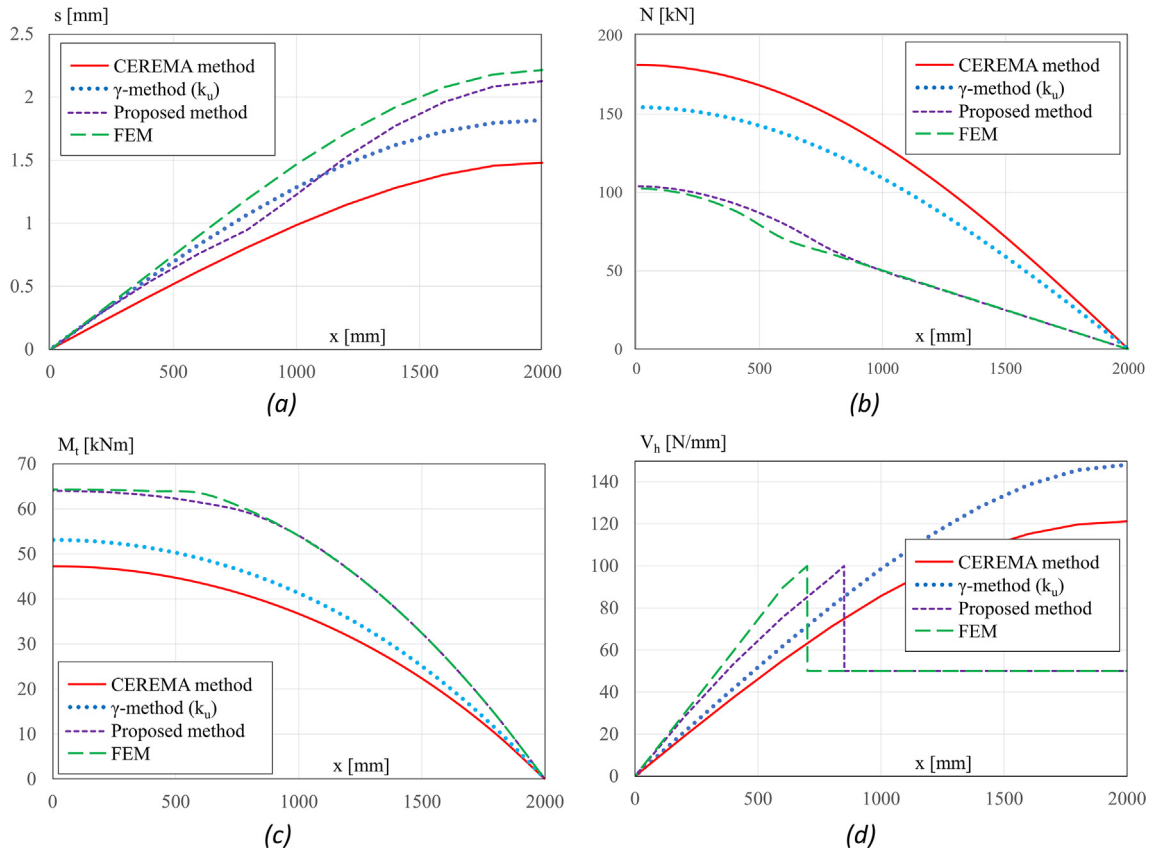
Fig. 7. Comparison of different methods in the plastic phase at $t = q/q_D = 148\%$ in terms of distribution of (a) slip s; (b) axial force N; (c) timber moment M_t and (d) shear flow V_h.

limits against the FEM solutions in terms of failure function φ, maximum slip s_{max}, maximum axial force N_{max} and maximum deflection in function of the applied load. The proposed method predicts well the FEM solutions. Note that the FEM solution and the proposed method tend to the asymptotic limits for high load levels ($t > 1$) while approaching the ductile failure.

4.2. Validation against non-linear push-over method [59]

Zhang presented a semi-analytical solution for TCC structures with perfectly elasto-plastic shear law based on superposition of linear calculations of the TCC structure after each connector yielding [59]. This method was called non-linear static push-over analysis in the works of Gauvreau [61]. For this comparison, we consider the case study proposed by Zhang of a simply supported beam subjected to uniform load with following parameters [59,59]: $L = 8000$ mm, $h_i = 0$ mm, $E_c = 42000$ N/mm^2, $h_c = 80$ mm, $b_c = 1000$ mm, $E_t = 12400$ N/mm^2, $h_t = 300$ mm, $b_t = 130$ mm, $V_{H0} = V_{Hr} = 40$ kN, $K = 100$ kN/mm, $l_{sp} = 500$ mm, The strengths of timber are assumed to be: $f_t^T = 30$ N/mm^2, $f_t^B = 45$ N/mm^2. The model parameters can be then calculated as follows: $h_d = 190$ mm, $EA_{con} = 3.36 \times 10^9$ N, $EA_{tim} = 4.84 \times 10^8$ N, $EA_h = 4.23 \times 10^8$ N, $EI_c = 1.79 \times 10^{12}$ Nmm^2, $EI_t = 3.63 \times 10^{12}$ Nmm^2, $EI_0 = 5.42 \times 10^{12}$ Nmm^2, $EI_\infty = 2.07 \times 10^{13}$ Nmm^2, $D_{e1} = -6.69 \times 10^{-5}$, $D_{e2} = 1.94 \times 10^{-5}$, $D_{e3} = 6.32 \times 10^{-2}$, $D_{e4} = 3.37 \times 10^4$, $\alpha = 4.75 \times 10^{-11}$, $\omega = 1.34 \times 10^{-3}$, $q_D = 6.33$ N/mm.

Fig. 9a compares the proposed method with the push-over method and FEM solution in terms of load vs. deflection. Moreover, the Frozen Shear Method [10] (FSM), which assumes that all connector plasticize simultaneously, is also compared. It is worth reminding that the FSM is simply a bilinear load–displacement curve which is composed by the linear response according to γ-method, followed by the unconnected beam stiffness after the plasticization of the external first connector.

As a result, the proposed solution is slightly stiffer than those of other methods in the elastic phase, but when the load increases to the plastic domain, the proposed method is well in agreement with FEM solutions and push-over method. It is interesting to note that all methods tend to the asymptotic linear solution of Eq. (63). Analogously, Fig. 9b compares the predicted maximum axial force of the proposed method. The push-over method reaches the asymptotic linear solution before the FEM and the proposed model because the connector system is modeled in a discrete manner (i.e., each discrete connector is plasticized one after another), while the proposed method and FEM is calculated with equivalent continuous connectors with spread stiffness. However, the proposed method has an important advantage as it avoids any iterative calculation and computation efforts. Finally, the FSM method does not capture well the transition from elastic-to-plastic domain due to the assumption of simultaneous plasticity of all connectors, which causes an underestimation of the structural response after the linear domain.

Fig. 9a and b show that the structural behavior of a ductile TCC with ductile connectors can be divided in three parts: (i) $t < 1$ ($q_0 < q_D$): initial elastic response when the beam behaves in a linear and elastic manner; (ii) $1 < t_{cr} < 3$ ($q_0 < q_D < 3q_0$) : transition non-linear response where the load–deflection is non-linear due to the gradual plastification of the connectors; (iii) $t > 3$ ($q_0 > 3q_D$) asymptotic linear response part where the connectors are all plastified and the deflection increases linearly with respect the load increment.

4.3. Parametric analysis on V_h-s behavior of connector

A parametric analysis is carried out to assess the sensitivity of the TCC structural response to the connector parameters of the simplified connector law k, V_{h0}, V_{hr} as shown in Fig. 1b. The ductile TCC beam of Fig. 5 is considered for this study, while the following connector

Table 1
Comparison for results by different methods for the case study of Fig. 5.

Method	End of elasticity at $q_0 = q_D$			Failure of the TCC beam at $\varphi = 1$				
	q_D [N/mm]	N_{max}^D [kN]	w_{max}^D [mm]	q_{cr} [N/mm]	M_{cr} [kNm]	N_{cr} [kN]	s_{cr} [mm]	w_{cr} [mm]
No composite action ($\gamma = 0$)	13.86 (−58.9%)	0 (−100.0%)	5.00 (−26.0%)	92.5 (−4.5%)	185.0 (−4.5%)	0 (−100.0%)	6.66 (−16.4%)	33.33 (−6.4%)
Full-composite action ($\gamma = 1$)		0 (−100.0%)		129.4 (+33.5%)	258.8 (+33.5%)	76.9 (−23.2%)	0 (−100.0%)	11.97 (−61.8%)
CEREMA method	33.75 (+0.06%)	122.4 (−0.7%)	6.76 (0.0%)	112.0 (+15.6%)	224.0 (+15.6%)	405.9 (+305.5%)	3.31 (−42.1%)	22.43 (−28.4%)
γ-method k_s	34.32 (+1.7%)	127.3 (−3.0%)	7.02 (+3.8%)	112.5 (+16.1%)	225.0 (+16.1%)	417.3 (+316.9%)	3.27 (−42.8%)	23.01 (−26.5%)
γ-method k_u	27.50 (−18.5%)	84.9 (−35.3%)	6.38 (−5.6%)	108.6 (−12.1%)	217.2 (−12.1%)	334.9 (+234.6%)	3.95 (−30.9%)	25.18 (−19.6%)
Proposed Method (PM)	33.75 (−0.06%)	133.3 (−1.6%)	6.40 (−5.3%)	97.3 (+0.4%)	194.6 (+0.4%)	100.7 (+0.6%)	5.42 (−5.2%)	31.41 (+0.3%)
FEM analysis	33.73	131.2	6.76	96.90	193.8	100.1	5.72	31.32

parameter have been considered: (i) $k = 25, 50, 100, 200$ and 400 N/mm^2, while $V_{h0} = 100$ N/mm, $V_{hr} = 100\% V_{h0}$; (ii) $V_{h0} = 50, 100, 150, 200$ and 250 kN/m, while $k = 100$ N/mm^2, $V_{hr} = 100\% V_{h0}$; (iii) $V_{hr} = 0\%, 25\%, 50\%, 75\%$ and 100% V_{h0}, while $k = 100$ N/mm^2, $V_{h0} = 100$ N/mm.

Fig. 10a, b and c show the effect of the connector stiffness ($k = 25, 50, 100, 200$ and 400 N/mm^2, while $V_{h0} = 100$ N/mm, $V_{hr} = 100\%$ V_{h0}) on the maximum slip, maximum load and the load–deflection curve, respectively. For a ductile TCC, the connector stiffness does not affect the ultimate load, but the deflection at lower load level. That is, once all connectors have plastified, the maximum load does not depend on the connector stiffness and it can be estimated by stress equilibrium in the mid-span section as described by the Frangi's method [42]. Furthermore, N_{max} tends to approach about 200kN which is an asymptotic value of axial force based on the asymptotic limit of Eq.(60), which depends on V_{hr} only. Moreover, the deflection at failure w_{max} of such ductile TCC structure does not depend on the connector stiffness k. This observation can be explained by the asymptotic limit of Eq.(63): when the load increases, the deflection function depends principally on load q_0 and V_{hr}.

Fig. 10d, e and f show the effect of the connector shear strength ($V_{h0} = 50, 100, 150, 200$ and 250 kN/m, while $k = 100$ N/mm^2, $V_{hr} = 100\% V_{h0}$) on the maximum slip, maximum load and the load--deflection curve, respectively. While the connector strength has no effect on the initial response, it strongly affects the s_{max}, N_{max} and q_0 at the TCC collapse.

The strength V_{h0} strongly affects the end-of-linearity (EOL) as shown in Fig. 10a. Generally, when V_{h0} increases, the axial force increases, while the slip and deflection decrease. In the plastic domain, the load–deflection response tends to have the same slope, which is shifted by the V_{h0} value. Interestingly, the ultimate deflection visibly reduces by increasing V_{h0} (Fig. 10f).

Fig. 10g, h and i show the effect of the connector residual shear strength ($V_{hr} = 0\%, 25\%, 50\%, 75\%$ and 100% V_{h0}, while $k = 100$ N/mm^2, $V_{h0} = 100$ N/mm) on the maximum slip, maximum load and the load–deflection curve, respectively. V_{hr} does not affect the initial linear response, but it affects strongly the composite action N_{max} and the ultimate load q_0 at collapse. In general, when V_{hr} increases, the load at failure and axial force increase while the slip and deflection decrease.

In general, based on the parametric results, the connector stiffness k has a major effect on the initial structural stiffness in the elastic domain, but its effect on both the ultimate load and maximum deflection is rather negligible. The connector strength V_{h0} does not affect the initial structural stiffness in the elastic domain, but it strongly affects the end-of-linearity (EOL) load and the ultimate load. Finally, the residual connector strength V_{hr} does not affect the initial structural response and the EOL load, but it significantly affects the ultimate load. Both V_{h0} and V_{hr} affect the non-linear structural response by mainly vertically shifting the load–displacement curve. Interestingly, the ultimate loads seem to lay on a line, which means that the ultimate load reduces somewhat linearly when both V_{h0} and V_{hr} decrease. Finally, Fig. 10e and 10f shows the advantage of the proposed method against the Frozen shear method [10]. For instance, for the higher connection strength V_{h0} as 250kN is higher, the composite action N_{max} is still increasing during loading and the load–deflection curve is rather parabolic and can not be simplified by a simple bilinear curve. Moreover, the FSM does neither consider the effect of the gradual plasticization of the connectors on the ultimate load (Fig. 10f) nor the effect of residual strength lower than V_{h0} (Fig. 10i).

5. Simplified design method for a ductile TCC structure

5.1. Closed-form solution

This section presents a simplified method for estimating the structural response of a TCC structure (in terms of axial force, slip, deflection
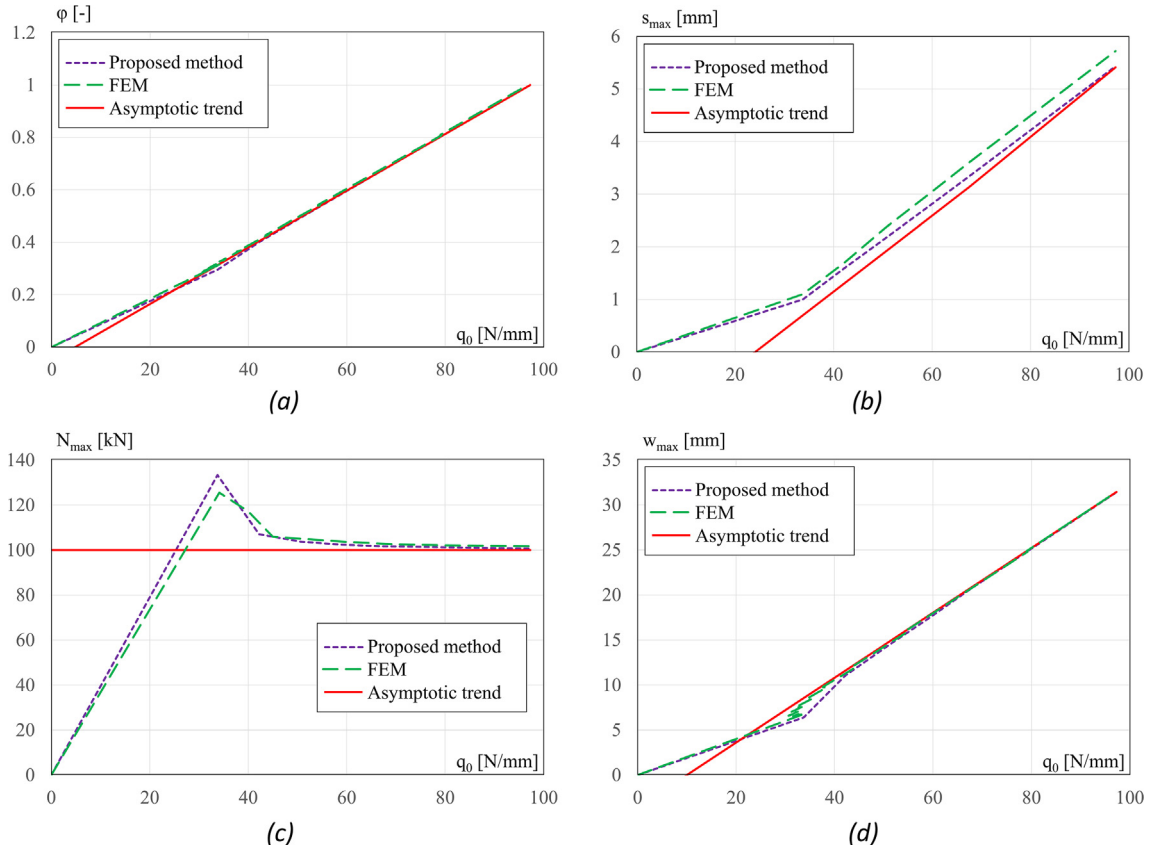
Fig. 8. For a ductile TCC structure, comparison of different methods in terms of: (a) failure function; (b) maximum slip; (c) maximum axial force; (d) deflection in function of the applied load t.

and failure criterion) directly from the connector parameters (k, V_{h0}, V_{hr}) for the assumed simplified shear law (GEP, EPP, BE) as shown in Fig. 1b.

First, we need to estimate the axial force and the failure function at different load levels t. The axial force N_{max} can be estimated as $N_{max}^E(q_0)$ by Eq. (36) in the elastic phase and as $N_{max}^P(t)$ by Eq. (55) for plastic phase, such as:

$$N_{\max}^E(q_0) = \frac{kLD_{e3}}{3}q_0 = D_{e4}q_0 \tag{64}$$

$$N_{\max}^P(t) = \frac{1}{2D_{e3}}\left\{[V_{hr}LD_{e3} - s_D D_{e4}(2t+1)]\sqrt{1 - \frac{1}{t}} + 2D_{e4}s_D t\right\} \tag{65}$$

The latter tends to the asymptotic limit N_{lim} and is described by Eq. (60) as $N_{\lim} = V_{hr}L/2$. The failure criterion φ is calculated directly by N_{max} and M_{max} by Eq. (58) as follows:

$$\varphi^P(t) = \frac{N_{\max}(t)}{A_t f_t^T} + [M_{\max}(t) - N_{\max}(t)h_d]\frac{E_t h_t}{2EI_0 f_t^B} \tag{66}$$

The values of N_{max} and φ can be calculated at any point of load q_0 (or t). Finally, the failure is reached when $\varphi = 1$. Similarly, the asymptotic φ_{lim} is found also by Eq. (61) as
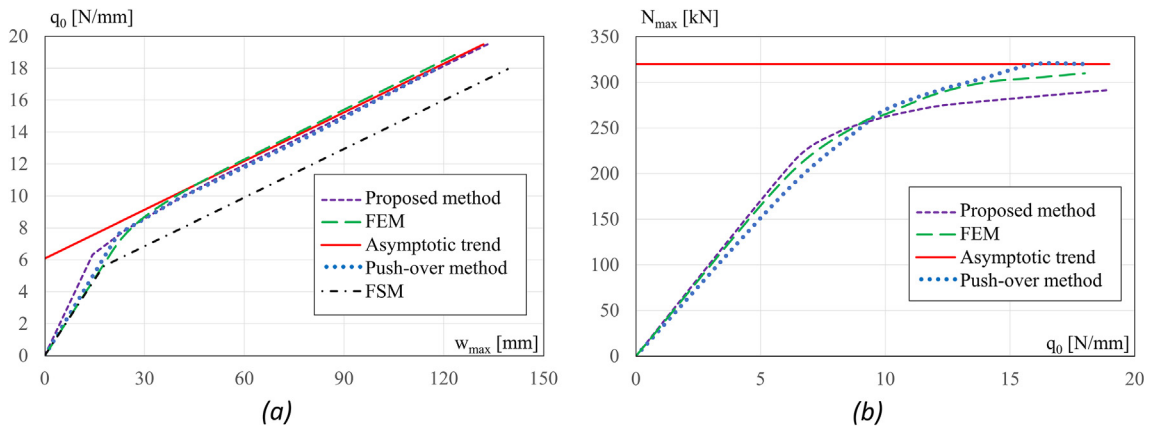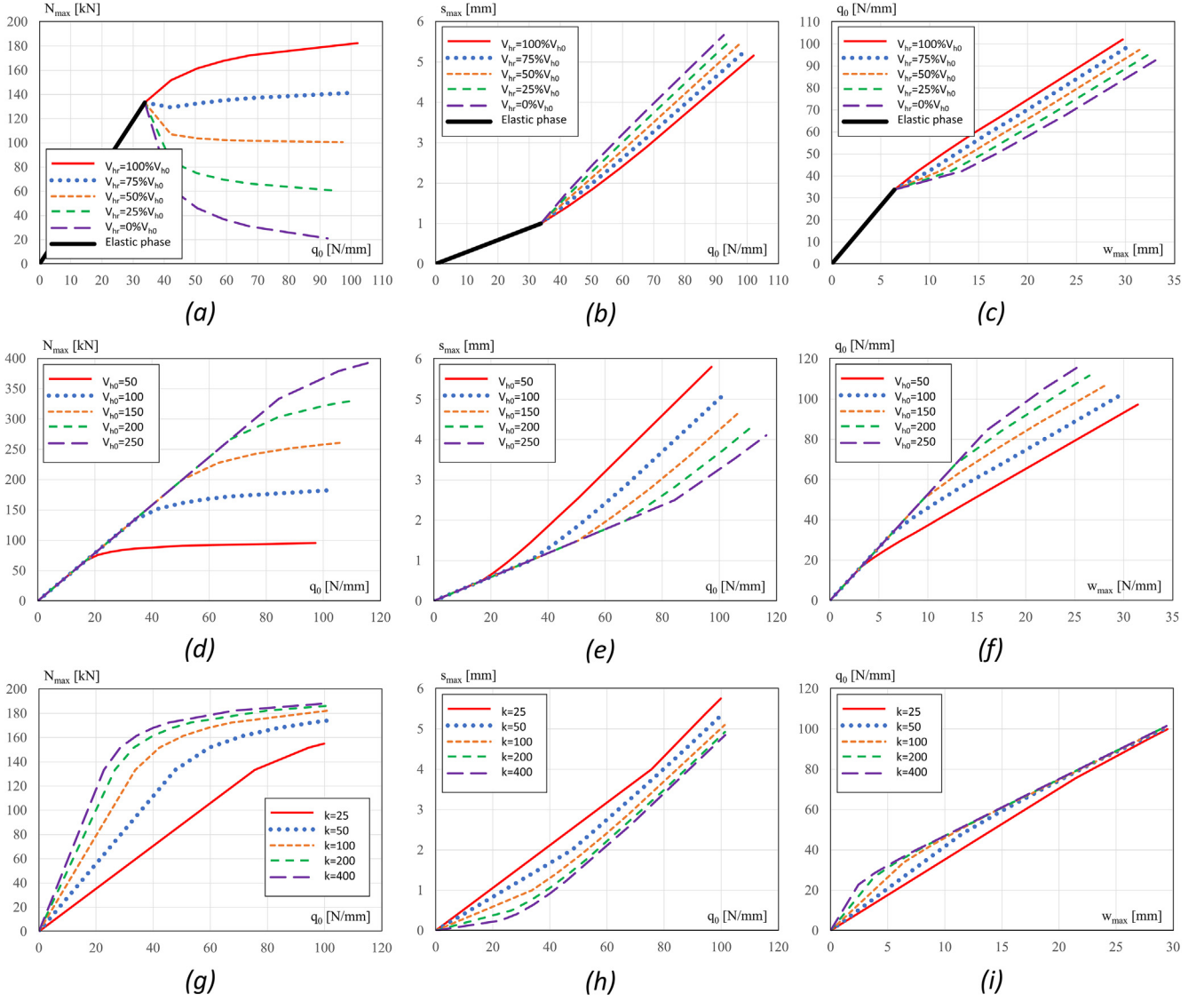

Fig. 9. Comparison of the proposed solution with push-over method [59,61] and FEM solution [60] in terms of (a): applied load vs. deflection; (b) maximum axial force vs. load.

Fig. 10. Parametric analysis on V_h-s behavior of connector. Influence of connector stiffness k on: (a) s_{max}, (b) N_{max} (c) q_0; influence of V_{h0} on (d) s_{max}, (e) N_{max}, (f) q_0; influence of ratio V_{hr}/V_{h0} (g) s_{max}, (h), N_{max} (i) q_0.

$$\varphi_{\lim} = \frac{L^2 E_t h_t}{16 E I_0 f_t^T} q_D t - \frac{L(EA_t h_d h_t f_t^T - 2 E I_0 f_t^B)}{4 A_t E I_0 f_t^T f_t^B} V_{hr}$$

$$= \frac{L^2 E_t h_t}{16 E I_0 f_t^T} q_0 - \frac{L(EA_t h_d h_t f_t^T - 2 E I_0 f_t^B)}{4 A_t E I_0 f_t^T f_t^B} V_{hr} \tag{67}$$

For the sake of simplicity, Table 2 reports the design values at loading levels $t = q_0/q_D$.

Then, the slip and the deflection at different load levels t are estimated. The slip function is the maximum value at the beam end ($x = L/2$). The function s_{max} is estimated to be $s_{max}^E(q_0)$ by Eq.(33) for the elastic phase and $s_{max}^P(t)$ by Eq.(52) for the plastic phase as follows:

$$s_{max}^E(q_0) = D_{e3} q_0 \tag{68}$$

$$s_{max}^P(t) = s_D + \frac{1}{48 D_{e3} E I_0} h_d L^3 s_D (t-1)\left(3 - \sqrt{1 - \frac{1}{t}}\right) - \frac{1}{8}\alpha V_{hr} h_d$$
$$L^2\left(1 - \frac{1}{t}\right) \tag{69}$$

Moreover, the asymptotic function s_{lim} is found by Eq. (62) as follows:

Table 2
Design tables for estimating the maximum axial force and failure function.

t [–]	x_D [mm]	q_0 [N/mm]	N_{max} [N]	M_{max} [N mm]
0	0.5L	0	0	0
1	0.5L	$q_D = \frac{s_0}{D_{e3}}$	$\frac{D_{e4}}{D_{e3}} s_0$	$\frac{L^2}{8} q_D$
1.25	0.276L	$1.25 q_D$	$\frac{0.467 D_{e4} s_0 + 0.223 V_{hr} L D_{e3}}{D_{e3}}$	$\frac{5L^2}{32} q_D$
1.5	0.211L	$1.5 q_D$	$\frac{0.345 D_{e4} s_0 + 0.287 V_{hr} L D_{e3}}{D_{e3}}$	$\frac{3L^2}{16} q_D$
1.75	0.173L	$1.75 q_D$	$\frac{0.277 D_{e4} s_0 + 0.327 V_{hr} L D_{e3}}{D_{e3}}$	$\frac{7L^2}{32} q_D$
2	0.146L	$2 q_D$	$\frac{0.232 D_{e4} s_0 + 0.353 V_{hr} L D_{e3}}{D_{e3}}$	$\frac{L^2}{4} q_D$
3	0.0915L	$3 q_D$	$\frac{0.142 D_{e4} s_0 + 0.408 V_{hr} L D_{e3}}{D_{e3}}$	$\frac{3L^2}{8} q_D$
6	0.0436L	$6 q_D$	$\frac{0.0663 D_{e4} s_0 + 0.456 V_{hr} L D_{e3}}{D_{e3}}$	$\frac{3L^2}{4} q_D$
10	0.0257L	$10 q_D$	$\frac{0.0388 D_{e4} s_0 + 0.474 V_{hr} L D_{e3}}{D_{e3}}$	$\frac{5L^2}{4} q_D$

$$s_{\lim} = s_D + \frac{h_d L^3 s_D (t - 0.75)}{24 D_{e3} E I_0} - \frac{1}{8} \alpha h_d L^2 V_{hr}$$

$$= s_D + \frac{h_d L^3}{24 E I_0}\left(q_0 - 0.75 \frac{s_D}{D_{e3}}\right) - \frac{1}{8} \alpha h_d L^2 V_{hr} \tag{70}$$

The maximum deflection w_{max} at mid-span ($x = 0$) is obtained analytically in the elastic phase by Eq. (39):

$$w_{\max}^E (q_0) = -\frac{L^2 (192 h_d D_{e4} - 25 L^2)}{1920 E I_0} q_0 \tag{71}$$

In the plastic phase, w_{max} is calculated from Eq.(57) and the expression is more lengthy as below:

$$w_{\max}(t) = \frac{2\sqrt{t(t-1)}}{375 t^2 (2t^2 - t - 1) D_{e3} E I_0} \cdot$$

$$\left\{ \begin{array}{l} \\ \\ \\ \\ \frac{625}{256}(2t + 1)t^2 \sqrt{t(t-1)} s_D L^4 \\ - \frac{125}{8}(t - 1)\left(t^2 + t + \frac{1}{4}\right) V_{hr} h_d D_{e3} L^3 \\ - \frac{75}{2}\left[\left(t + \frac{1}{2}\right)t^2 \sqrt{t(t-1)} - \left(t + \frac{1}{2}\right)(t - 1)\left(t^2 + \frac{1}{2}t + \frac{3}{8}\right)\right] D_{e4} h_d s_D L^2 \end{array} \right\} \tag{72}$$

An asymptotic function w_{lim} is found by Eq. (63) when the load increases.

$$w_{\lim} = \frac{5 L^4}{384 E I_0} \frac{s_D}{D_{e3}} t - \frac{L^3 h_d}{24 E I_0} V_{hr} = \frac{5 L^4}{384 E I_0} q_0 - \frac{L^3 h_d}{24 E I_0} V_{hr} \tag{73}$$

Table 3 summarizes the maximum slip and maximum deflection at different load levels $t = q_0 / q_D$. The ductility of the structure can be easily estimated by $\mu = w_{cr}/w_D$ where $w_D = w_{max}(t = 1)$ and $w_{cr} = w_{max}(t = t_{cr})$, which can be easily calculated from Table 3.

The model applicability is limited to TCC beams with connectors with a ductile shear law which is similar to the ones shown in Fig. 1b. By considering the experimental connector shear law (V_h-s), one should verify that the elasto-plastic connector law (Fig. 1b) is still valid up to the maximum slip (s_{max}) which corresponds to the ultimate load of the TCC beam.

5.2. Design procedure

The input variables needed for predicting the structural behaviour of TCC structure are:

- the connector parameters (k, s_D and V_{hr}) describing one of the 3 possible simplified shear laws (GEP, EPP, BE) as shown in Fig. 1b;
- the material properties (Young's modulus of concrete and timber E_c, E_t) and the timber strength under tension and bending (f_t^T, f_t^B);
- the geometrical parameters (inertia and areas I_c, A_c, I_t, A_c) and distance of the centroid of mass of the two sections h_d.

Based on these data, it is possible to estimate the coefficients D_{e1} and D_{e2} from Eqs. (29), D_{e3} from Eq.(31) and D_{e4} from Eq. (37). The latter coefficient depends on the connection stiffness k. Finally, q_D is calculated from Eq.(40) in function of the connector parameter s_D and D_{e3}.

Given the input variables, it is then possible to estimate the structural response of a TCC structure in terms of deflection, slip and axial force at different loading levels by Table 2 and Table 3. In summary, the TCC structural response can be estimated by the following step-by-step procedure:

(1) Calculate the maximum axial force N_{max} and failure function φ from Table 2 at different load levels t;
(2) Calculate the maximum slip s_{max} and maximum deflection w_{max} from Table 3 at different load levels t;
(3) Identify the critical load level $t = t_{cr}$ at failure ($\varphi = 1$) by linear interpolation;
(4) If $t_{cr} < 1$ (failure in the elastic phase), it is possible using linear analytical methods such as the γ–method;
(5) If $1 < t_{cr} < 3$ (failure in the non-linear transition response), interpolate the values of N_{max}, s_{max}, w_{max} at failure (N_{cr}, s_{cr}, w_{cr}) by using q_{cr} and t_{cr}.
(6) If $t_{cr} > 3$ (failure in asymptotic part), it is possible to calculate the values of N_{cr}, s_{cr}, w_{cr} by using the asymptotic functions.

As schematically illustrated in Fig. 11, the structural response of a TCC structure with ductile connectors (as the ones assumed in Fig. 1b) shows three different domains: (i) the initial elastic domain (i.e., timber breaks in tension before any connectors yield); (ii) the nonlinear response with moderate structural ductility during the transition between the elastic and asymptoti behaviour (i.e., timber breaks in tension while connectors have started to yield); (iii) the final asymptotic response with high structural ductility (i.e., timber breaks in tension after all connectors have yielded). Notably, one can use the proposed design procedure not only for predicting the structural response, but also for assuring that the designed TCC structure has the desired structural ductility.
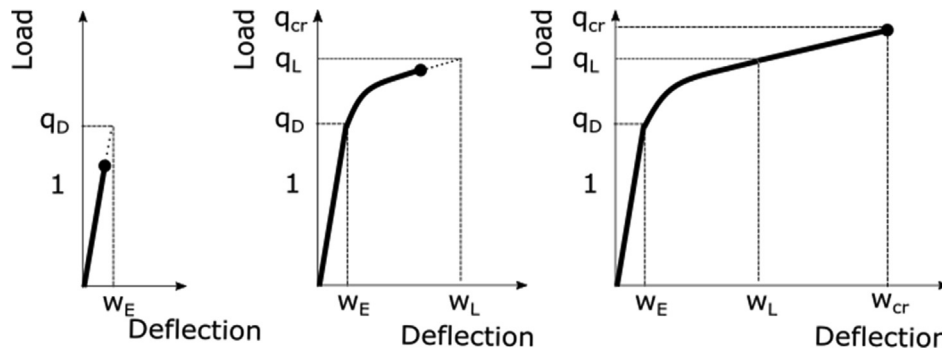
Table 3
Design tables for predicting the maximum slip and maximum deflection.

t [–]	x_D [mm]	q_0 [N/mm]	s_{max} [mm]	w_{max} [mm]
0	0.5L	0	0	0
1	0.5L	$q_D = \frac{s_D}{D_{e3}}$	s_D	$-\frac{L^2(192 d D_{e4} - 25 L^2)}{1920 E I_0}\frac{s_0}{D_{e3}}$
1.25	0.276L	$1.25 q_D$	$s_D + 0.0133 \frac{d s_0 L^3}{E I_0 D_{e3}} - 0.025 \alpha d V_{hr} L^2$	$\frac{0.0163 s_0 L^4 - 0.0261 V_{hr} d D_{e3} L^3 - 0.0333 D_{e4} d s_0 L^2}{E I_0 D_{e3}}$
1.5	0.211L	$1.5 q_D$	$s_D + 0.0252 \frac{d s_0 L^3}{E I_0 D_{e3}} - 0.0417 \alpha d V_{hr} L^2$	$\frac{0.0195 s_0 L^4 - 0.0321 V_{hr} d D_{e3} L^3 - 0.0201 D_{e4} d s_0 L^2}{E I_0 D_{e3}}$
1.75	0.173L	$1.75 q_D$	$s_0 + 0.0366 \frac{d s_0 L^3}{E I_0 D_{e3}} - 0.0536 \alpha d V_{hr} L^2$	$\frac{0.0227 s_0 L^4 - 0.0351 V_{hr} d D_{e3} L^3 - 0.0137 D_{e4} d s_0 L^2}{E I_0 D_{e3}}$
2	0.146L	$2 q_D$	$s_0 + 0.0478 \frac{d s_0 L^3}{E I_0 D_{e3}} - 0.0625 \alpha d V_{hr} L^2$	$\frac{0.0260 s_0 L^4 - 0.0368 V_{hr} d D_{e3} L^3 - 0.00997 D_{e4} d s_0 L^2}{E I_0 D_{e3}}$
3	0.0915L	$3 q_D$	$s_0 + 0.0910 \frac{d s_0 L^3}{E I_0 D_{e3}} - 0.0833 \alpha d V_{hr} L^2$	$\frac{0.0391 s_0 L^4 - 0.0397 V_{hr} d D_{e3} L^3 - 0.00402 D_{e4} d s_0 L^2}{E I_0 D_{e3}}$
6	0.0436L	$6 q_D$	$s_0 + 0.217 \frac{d s_0 L^3}{E I_0 D_{e3}} - 0.104 \alpha d V_{hr} L^2$	$\frac{0.0781 s_0 L^4 - 0.0412 V_{hr} d D_{e3} L^3 - 0.000928 D_{e4} d s_0 L^2}{E I_0 D_{e3}}$
10	0.0257L	$10 q_D$	$s_0 + 0.385 \frac{d s_0 L^3}{E I_0 D_{e3}} - 0.113 \alpha d V_{hr} L^2$	$\frac{0.130 s_0 L^4 - 0.0415 V_{hr} d D_{e3} L^3 - 0.000325 D_{e4} d s_0 L^2}{E I_0 D_{e3}}$

Fig. 11. Possible modes of structural behavior of a TCC structure with elastic beams and ductile connectors as shown in Fig. 1b.

Table 4
Mechanical properties of the considered concrete kinds.

Property	UHPFRC	HPC	NC
Elastic modulus E_c [GPa]	50	31.2	23.4
Compressive strength f_c^C [MPa]	140	60	30.2
Tensile strength f_c^T [MPa]	8	4.6	2.9

5.3. Statistical validation

This section aims at carrying out a wide range validation of the proposed procedure for TCC structures with different beam span, timber and concrete section, concrete kind, connector stiffness, etc. The configurations were chosen arbitrarily by selecting a very wide range of parameters for residential floor system, which consider the current construction practise in Canada and future trends. The parameters of the composite beam are determined as follows:

(1) Span: L = 4000, 8000, 12,000 [mm]
(2) Concrete kind: we consider some typical values for 3 classes of concretes UHPFRC Ductal JS 1000 [62], HPC King HP-S10 [63], Normal concrete NC [64] which present the mechanical characteristics as follows Table 4:

Height of concrete slab: the slab thickness is assumed for each kind of concrete is assumed to have a similar flexural stiffness, such as h_c^{NC}: h_c^{HPC}: h_c^{UHPFRC} = 1.0: 0.9: 0.8 where h_c^{NC} = $L/80$;

(3) The width of the timber b_t is chosen to have the following range of ratio EI_t/EI_c = 2, 4, 8 respectively.
(4) Composite degree of Y = 0.2, 0.5, 0.8, which are respectively low, average and high degree of composite, respectively. The composite

degree Y is a parameter for evaluating the composite action in terms of flexural stiffness as $Y = (EI_{eff} - EI_0)/(EI_\infty - EI_0)$. The composite degree Y expressed the composite action in terms of the effective bending stiffness EI_{eff} of the composite beam, while γ represents a non-dimensional factor for the composite action for which $EI_{eff} = EI_0$ for $\gamma = 0$ and $EI_{eff} = EI_\infty$ for $\gamma = 1$.

The effective concrete slab width b_c is determined in CSA A23.3–14 [65] and CSA S16-14 [66] as $b_c = \min(L/4, 24h_c, b_2)$ where b_2 is the timber spacing. In this case, we assumed that the effective width is determined by the span such as $b_c = L/4$. The height of timber beam is fixed $L/20$ to minimize the effect of timber shear on the deflection; For the timber we choose typical value for Glulam from a commercial database (i.e., Nordic Lam 24F-ES/NPG [67]) which presents elastic modulus E_t = 13.1 GPa and average strength f_t^T = 30.6 MPa, f_t^B = 46.1 MPa, f_t^C = 50.5 MPa.

As for the choice of a ductile connector, the experimental shear behaviour of notch connectors with steel fasteners as shown in Fig. 12a is considered from [16]. As shown in the same figure, two possible shear laws GEP1 and GEP2 have been investigated to simplify the experimental shear law. The structural response predicted by the experimental shear law and the simplified shear laws GEP1 and GEP2 is compared with FEM analysis. The accuracy of the simplified shear law GEP to reproduce the structural response of the experimental shear law is rather satisfactory.

Based on the combination of the considered parameters, 81 possible TCC beams were analyzed. The collapse failure is always assumed to be the lower fiber of timber beam under combination of bending and tensile solicitation. Based on the proposed method, 22% TCC beams collapse in the elastic phase (t_{cr} < 1), 56% TCC beams collapse in the non-linear transition part with moderate ductility (1 < t_{cr} < 3), and 22% TCC beams collapse in the asymptotic linear phase with enhanced structural ductility (t_{cr} > 3). This demonstrates the importance to have
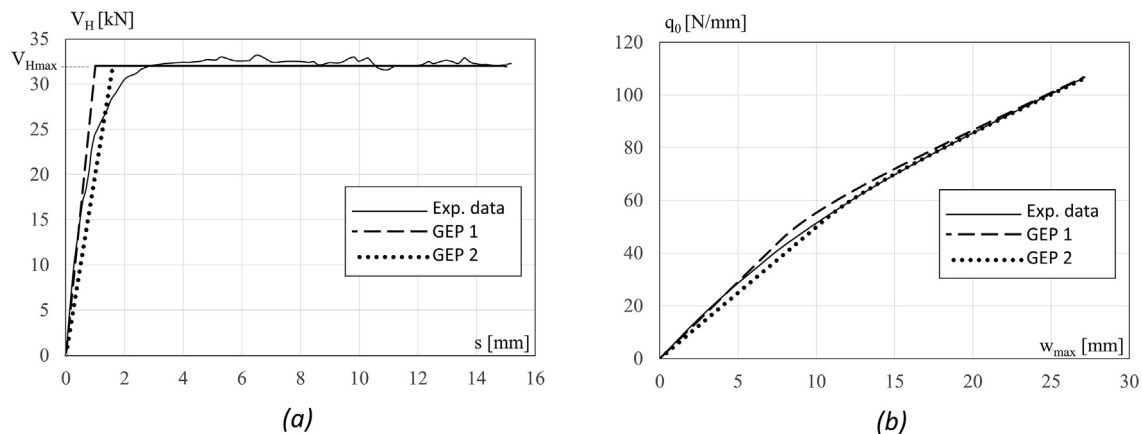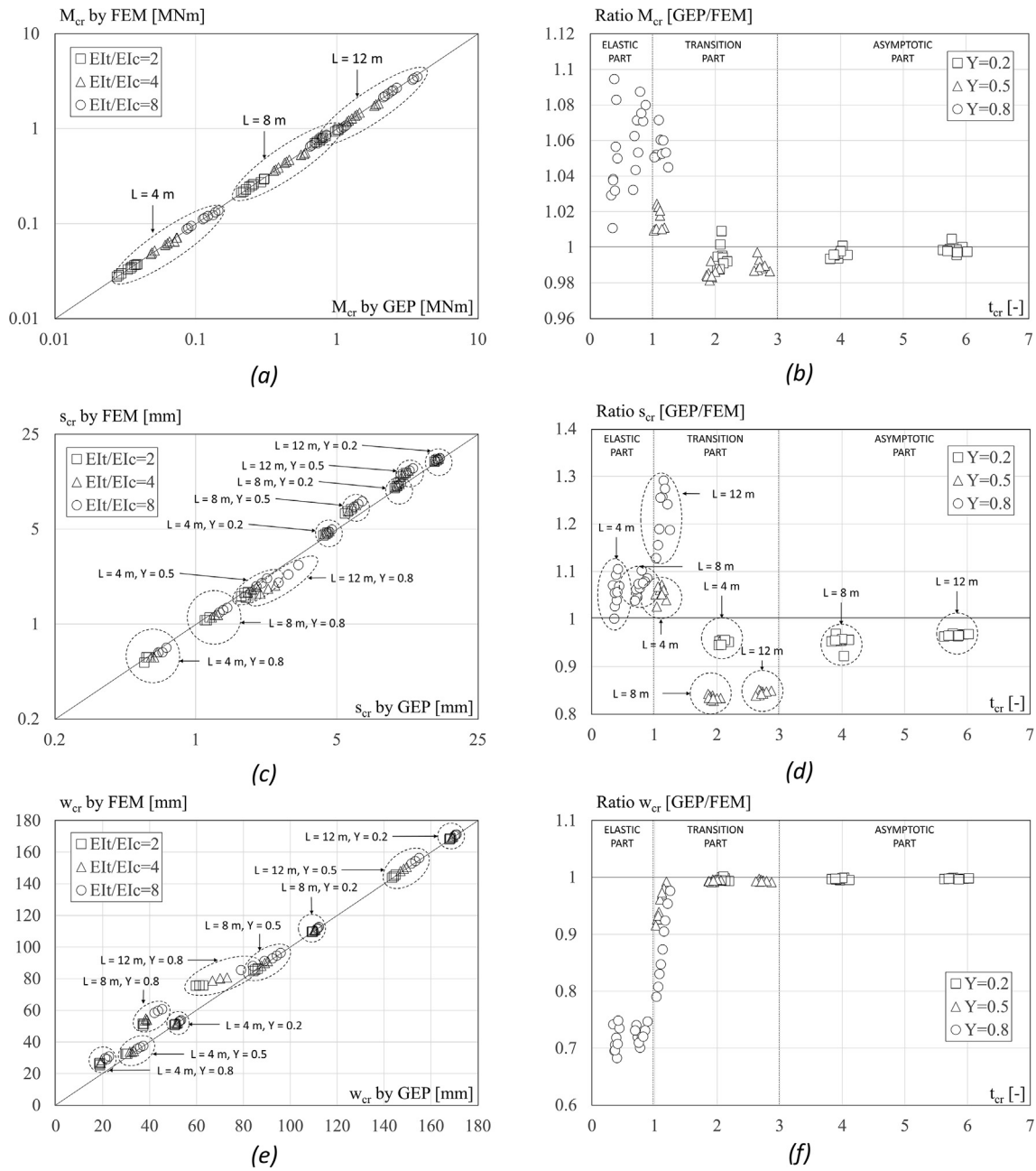

Fig. 12. Comparison of the experimental connector law and simplified GEP for the proposed model.

Fig. 13. Comparison of proposed method GEP vs. FEM solution for all 81 TCC cases without concrete crack for: (a, b) maximum moment M_{cr} (c, d) ultimate deflection w_{cr}; (e, f) ultimate slip s_{cr}.

a simplified model to predict also a possible failure in the transition regime while connectors yield gradually.

5.3.1. Without concrete slab cracking

Fig. 13a, c, and e compare the prediction accuracy of the proposed model against FEM analyses for the proposed connector law for the maximum moment M_{cr}, maximum deflection w_{cr}, and maximum slip s_{cr}, respectively. Analogously, Fig. 13b, d, and f show the ratio between the GEP and FEM variable. In spite of the model simplicity, its accuracy is satisfactory especially beyond the limit of elasticity. Fig. 13b shows that the moment M_{cr} is well predicted for both ranges in which the connectors start to yield (transition zone $1 < t < 3$) and all yield (asymptotic range $t > 3$). Fig. 13b shows that the maximum error in the prediction of the critical moment is about 10% in the elastic domain and 2% in the plastic domains. Fig. 13d shows that the GEP model predicts less precisely the ultimate slip with an error of 20–30% in the

elastic domain, which reduces to 10–15% in the plastic domain. Nevertheless, Fig. 13e shows that the simplified GEP model predicts also the maximum deflection w_{cr} in the plastic domain with good accuracy. However, the prediction of the maximum deflection of the brittle TCC beams which collapse in the elastic domain is less satisfactory with an error of about 30%.

It is interesting to notice from Fig. 13b that connectors with a high composite degree Y failed in the elastic regime. This is due to the fact that when the connection stiffness is very high, the connection strength it is also very high and not achieved by the structure at collapse. On the critical moment M_{cr}, the Fig. 13 (a) and (b) shows that the span length L is dominant factor. At a given value of L, the ratio EI_t/EI_c takes influence by significantly increasing the M_{cr}. while ratio Y plays only a major role in the failure type. The ratio EIt/EIc has less influence on w_{cr}. On the critical slip w_{cr}, the Fig. 13 (c) and (d) shows that ratio Y becomes the dominant factor when $Y = 0.8$ leads a small critical slip despite L. The
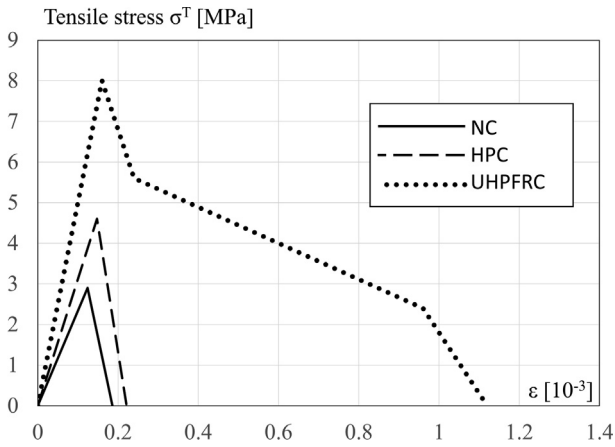
Fig. 14. Tensile stress-strain relationship assumed for NC, HPC and UHPFRC.

Table 5
Adjustment factors for cracking concrete.

Predicted variable	Transition response $1 < t < 3$	Asymptotic response $t > 3$
M_{cr}	0.85	0.75 for $EI_t/EI_c < 3$
		0.85 for $EI_t/EI_c > 4$
		0.9 for $EI_t/EI_c > 6$
w_{cr}	1.05	1.05
s_{cr}	1.25	1.15

span length only shows the influence when Y decreases to 0.5 and 0.2. On the critical deflection w_{cr}, the Fig. 13 (e) and (f) shows that L is still most important factor while ratio Y also take a significant role.

5.3.2. Accounting for concrete slab cracking

The contribution of the concrete moment is often secondary with respect to the timber and composite moments for a TCC structure. However, the reduction of the concrete section by a upward translation of the neutral axis may reduce the moment contribution due to the composite action [39]. Schanak et al. showed that the importance of the concrete slab cracking is relevant only for TCC slab with rather low EI_t/EI_c ratios, i.e., with rather thick concrete slab [68]. Although the proposed model does not account the effect of possible cracking of the concrete slab, this section aims at assessing the error of the model

prediction in the case of slab concrete cracking. Thus, the 81 cases of TCC beams were analyzed with non-linear FEM analysis [39] taking into account typical tensile stress–strain relationship for the 3 kind of concretes as Fig. 14.

Fig. 15 compares the results in terms of M_{cr}, s_{cr} and w_{cr} for the proposed GEP model and the FEM analysis with concrete cracking. The proposed model can overestimate the M_{cr} of ductile TCC beams with low EI_t/EI_c ratio of 2 can be up to 30%. However, for TCC beam with more conventional EI_t/EI_c ratio of 4 and 8, the error reduces to 10–15%. It is also interesting to notice that the error is much reduced in the case of UHPFRC concrete as the tensile strength reduces the uplift of the neutral axis and the loss of composite action. Interestingly, the proposed model well predicts the critical deflection of ductile TCC structures.

Based on the statistical analysis in section Table 5 proposes adjustment factors for accounting for the effect of concrete cracking on predicting M_{cr} (or q_{cr}), w_{cr}, s_{cr} at the structural failure with the effect of slab concrete cracking.
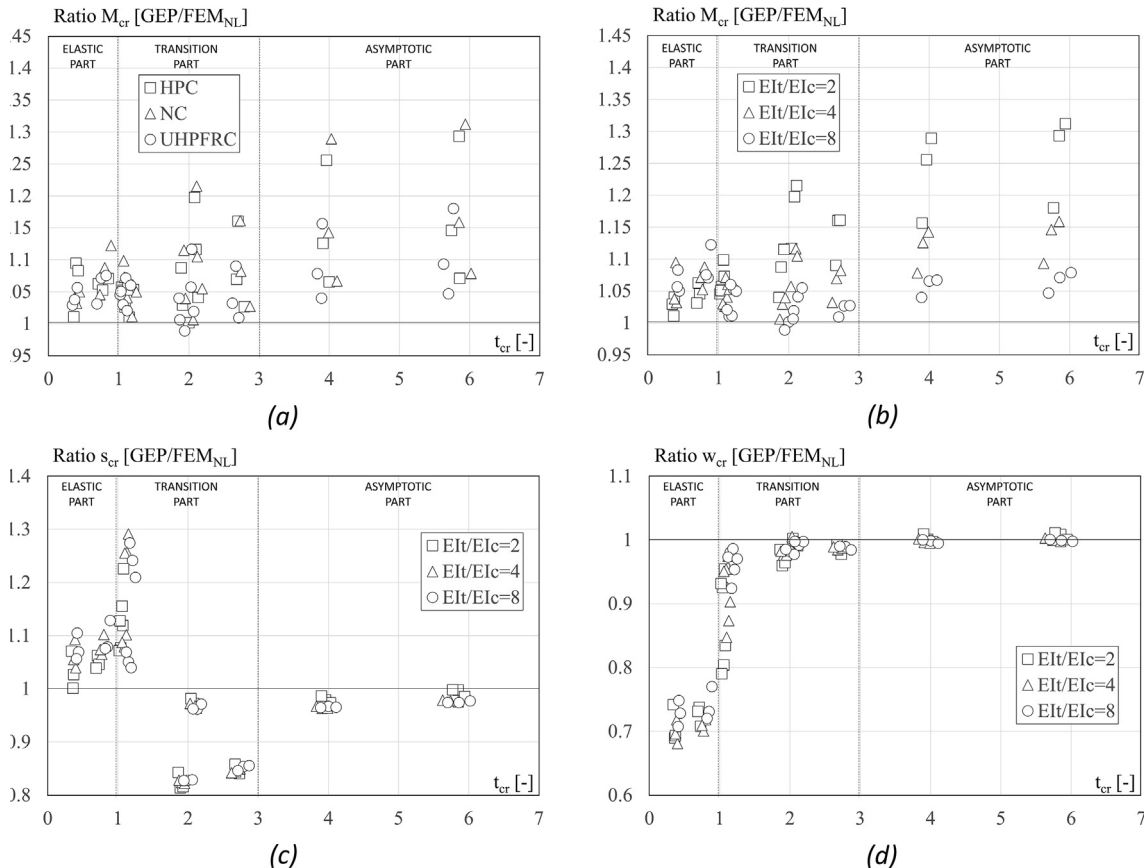

Fig. 15. Comparison of proposed method GEP vs. FEM solution for all 81 TCC cases with concrete crack for: (a), (b) M_{cr}; (c) s_{cr}; (d) w_{cr}.

6. Concluding remarks

This work proposes an analytical closed-form solution for predicting the structural response of a TCC structures with ductile shear connectors. Based on the presented results, the following conclusions can be drawn:

(1) It was possible to obtain an analytical solution of the method proposed by Bažant and Vitek and Baby assuming an approximate slip distribution for the plastic domain and a simplified shear law, such as, Generalized Elasto-Plastic (GEP), Perfectly Elasto-Plastic (PEP) or Brittle-Elastic (BE) as shown in Fig. 1b:

(2) The goodness of the approximate solution in predicting the full structural response of the TCC structure was validated against linear methods and numerical FEM analysis in both linear elastic and plastic domain. The proposed method slightly underestimates the elastic response, but it well predicts the structural response of the TCC beam when the connectors gradually yield. In particular, the proposed method provides a better estimation of the inelastic structural response and ultimate load than the Frozen Shear Method (which assumes a simultaneous plasticization of the connectors);

(3) It was found by proposed method that the a plastically designed TCC structure with elasto-plastic shear law tends to a linear asymptotic structural response when all the connectors have yielded;

(4) A simplified point-to-point method (based on Tables 2 and 3) has been proposed for predicting the structural response in terms of deflection, slip and moment at different load levels directly from the 3 parameters of the connector shear law and the materials' property. Notably, the analytical proposed model can be employed to design TCC structures with a desired structural ductility;

(5) Based on the parametric analysis on different TCC beams, the robustness of the proposed method in predicting the maximum moment, deflection and slip of ductile TCC structure has been validated. Note that the proposed model is not meant for predicting the structural response of a brittle TCC structure with a timber collapse before the connector yielding, for which the γ-methot is still recommended;

(6) The effect of concrete cracking on the prediction of the TCC structural response of the proposed model has been verified by nonlinear FEM. This effect is particular important for TCC structure with $(EI)_c/(EI)_t$ lower than 4 and a correction factor has been proposed. When a UHPFRC slab is employed, the model prediction for the ultimate moment is fairly satisfactory as the tensile strength reduces the loss of composite action.

Future works shall focus on the following improvements or model extensions, such as: (i) continuous TCC beams; (ii) non-uniform distribution of ductile connectors; (iii) the effect of possible uplifts between timber and concrete in proximity of the supports at failure load; (iv) a statistical study on the effect of the variability of material property on the predicted structural response to assure that the ductile connection failure always occurs before the timber failure; (v) the proposed shear law should be generalized with a softening brunch to account for more general connector law.

CRediT authorship contribution statement

Truong-Thanh Nguyen: Conceptualization, Data curation, Formal analysis, Investigation, Methodology, Software, Validation, Visualization, Writing - original draft. **Luca Sorelli:** Conceptualization, Funding acquisition, Project administration, Supervision, Writing - review & editing. **Eugen Brühwiler:** Conceptualization, Funding acquisition, Project administration, Supervision, Writing - review & editing.

Declaration of Competing Interest

The authors declare that they have no known competing financial interests or personal relationships that could have appeared to influence the work reported in this paper.

Acknowledgements

Appendix A. Supplementary material

Supplementary data to this article can be found online at https://doi.org/10.1016/j.engstruct.2020.110826.

References

[1] Ceccotti A. Composite concrete-timber structures. Prog Struct Eng Mater 2002;4(3):264–75.

[2] Yeoh D, Fragiacomo M, De Franceschi M, Heng Boon K. State of the art on timber-concrete composite structures: Literature review. J Struct Eng 2010;137(10):1085–95.

[3] Le Roy R, Pham HS, Foret G. New wood composite bridges. Eur J Environ Civ Eng 2009;13(9):1125–39.

[4] Dias A, Skinner J, Crews K, Tannert T. Timber-concrete-composites increasing the use of timber in construction. Eur J Wood Wood Prod 2016;74(3):443–51.

[5] Grantham R, Enjily V, Fragiacomo M, Nogarol C, Zidaric I, Amadio C. Potential upgrade of timber frame buildings in the UK using timber-concrete composites. In: Proceedings of the 8th World Conference on Timber Engineering, vol. 2; 2004, pp. 59–64.

[6] Wacker JP, Dias AMPG, Hosteng TK. 100 years performance of timber-concrete-composite bridges in the USA. ASCE J Bridge Eng 2019.

[7] Zingg S, Habert G, Lämmlein T, Lura P, Denarié E, Hajiesmaeili A. Environmental assessment of radical innovation in concrete structures. Expand Boundaries Syst Think Built Environ 2016.

[8] Rodrigues JN, Providência P, Dias AM. Sustainability and lifecycle assessment of timber-concrete composite bridges. J Infrastruct Syst 2016;23(1):04016025.

[9] Martins C, Dias AM, Costa R, Santos P. Environmentally friendly high performance timber–concrete panel. Constr Build Mater 2016;102:1060–9.

[10] van der Linden ML. Timber-concrete composite beams. HERON-Engl Ed 1999;44(3):215–36.

[11] McCullough CB. Oregon tests on composite (Timber-Concrete) beams (TIMBER-CONCRETE) BEAMS. J Proc 1943;39:429–40.

[12] Dias AM, Ferreira MC, Jorge LF, Martins HM. Timber–concrete practical applications–bridge case study. Proc Inst Civ Eng-Struct Build 2011;164(2):131–41.

[13] Naud N, Sorelli L, Salenikovich A, Auclair-Cuerrier. A new UHPFRC-Glulam Laminated Timber composite floors for multi-storey buildings. Elsevier, Engineering Structures, accepted with minor correction 2018.

[14] Dias AMPG. Mechanical behaviour of timber-concrete joints. Universidade de Coimbra, Portugal; 2005.

[15] Cuerrier-Auclair S, Dagenais C, Hu L, Gagnon S. Technical design guide for timber-concrete composite floors in Canada. FPInnovations 2018.

[16] Dias A, Martins ARD, Simões LMC, Providência PM, Andrade AAM. Statistical analysis of timber–concrete connections–Mechanical properties. Comput Struct 2015;155:67–84.

[17] Dias A. Analysis of the nonlinear behavior of timber-concrete connections. J Struct Eng 2011;138(9):1128–37.

[18] Gelfi P, Giuriani E, Marini A. Stud shear connection design for composite concrete slab and wood beams. J Struct Eng 2002;128(12):1544–50.

[19] Lukaszewska E, Johnsson H, Fragiacomo M. Performance of connections for prefabricated timber–concrete composite floors. Mater Struct 2008;41(9):1533–50.

[20] Deam BL, Fragiacomo M, Buchanan AH. Connections for composite concrete slab and LVL flooring systems. Mater Struct 2008;41(3):495–507.

[21] Khorsandnia N, Valipour HR, Crews K. Experimental and analytical investigation of short-term behaviour of LVL–concrete composite connections and beams. Constr Build Mater 2012;37:229–38.

[22] Selçukoglu E, Zwicky D. Towards the plastic design of glulam concrete composite structures. In: IABSE Symposium Report, vol. 96; 2009, pp. 20–29.

[23] Gutkowski RM, Brown K, Shigidi A, Natterer J. Investigation of notched composite wood–concrete connections. J Struct Eng 2004;130(10):1553–61.

[24] Yeoh D, Fragiacomo M, Aldi P, Mazzilli M, Kuhlmann U. Performance of notched coach screw connection for timber-concrete composite floor system; 2008.

[25] Dias AM, Kuhlmann U, Kudla K, Mönch S, Dias AMA. Performance of dowel-type fasteners and notches for hybrid timber structures. Eng Struct 2018;171:40–6.

[26] Yeoh D, Fragiacomo M, De Franceschi M, Buchanan AH. Experimental tests of notched and plate connectors for LVL-concrete composite beams. J Struct Eng 2010;137(2):261–9.

[27] Monteiro SRS, Dias A, Negrão J. Assessment of timber—concrete connections made with glued notches: Test set-up and numerical modeling. Exp Tech 2013;37(2):50–65.

[28] Bathon L, Graf M. A continuous wood-concrete-composite system. In: Proc., World Conference of Timber Engineering, Whistler, BC; 2000.

[29] Gerber AR. Timber-concrete composite connectors in flat-plate engineered wood products. 2016. p. 163.

[30] Clouston P, Bathon LA, Schreyer A. Shear and bending performance of a novel wood–concrete composite system. J Struct Eng 2005;131(9):1404–12.

[31] Auclair SC, Sorelli L, Salenikovich A. A new composite connector for timber-concrete composite structures. Constr Build Mater Jun. 2016;112:84–92. https://doi.org/10.1016/j.conbuildmat.2016.02.025.

[32] Pirinen M. Ductility of wood and wood members connected with mechanical fasteners; 2014.

[33] Jiang Y, Crocetti R. CLT-concrete composite floors with notched shear connectors. Constr Build Mater 2019;195:127–39.

[34] Dias AM, Jorge LF. The effect of ductile connectors on the behaviour of timber–concrete composite beams. Eng Struct 2011;33(11):3033–42.

[35] Zhang C, Gauvreau P. Timber-concrete composite systems with ductile connections. J Struct Eng 2014;141(7):04014179.

[36] Pluess Y, Zwicky D. Plastic design of timber concrete composite girders. London: IABSE/IASS; 2011.

[37] Ceccotti A, Fragiacomo M, Gutkowski RM. Design of timber-concrete composite structures according to EC5-2002 version. In: Meeting thirty-five of the Working Commission W18-Timber Structures, CIB; 2002.

[38] B. EN, 2: 2004 Eurocode 5: Design of timber structures–Part 2: Bridges. BSI, London; 1995.

[39] Auclair SC, Sorelli L, Salenikovich A. Simplified nonlinear model for timber-concrete composite beams. Int J Mech Sci Oct. 2016;117:30–42. https://doi.org/10.1016/j.ijmecsci.2016.07.019.

[40] Salari MR, Spacone E, Shing PB, Frangopol DM. Nonlinear analysis of composite beams with deformable shear connectors. J Struct Eng 1998;124(10):1148–58.

[41] Bazant ZP, Vítek JL. Compound size effect in composite beams with softening connectors. I: Energy approach. J Eng Mech 1999;125(11):1308–14. https://doi.org/10.1061/(ASCE)0733-9399(1999)125:11(1308).

[42] Frangi A, Fontana M. Elasto-plastic model for timber-concrete composite beams with ductile connection. Struct. Eng. Int. 2003;13(1):47–57.

[43] Boccadoro L, Zweidler S, Steiger R, Frangi A. Calculation model to assess the structural behavior of LVL-concrete composite members with ductile notched connection. Eng Struct 2017;153:106–17.

[44] Stüssi F. Beiträge zur Berechnung und Ausbildung zusammengesetzter Vollwandträger. Schweiz. Bauztg. 1943; 121.

[45] Newmark NM, Siess CP, Viest IM. Test and analysis of composite beams in complete interaction. Proc Soc Exp Stress Anal 1951;9:75–92.

[46] Pleshkov PF. Theoretical studies of composite wood structures. Sov Union Russ 1952.

[47] Gelfi P, Giuriani E. Influence of slab-beam slip on the deflection of composite beams. Int J Restor Build Monum 2003;9(5):475–90.

[48] Girhammar UA, Pan DH. Exact static analysis of partially composite beams and beam-columns. Int J Mech Sci 2007;49(2):239–55. https://doi.org/10.1016/j.ijmecsci.2006.07.005.

[49] Dias A, Van de Kuilen JW, Lopes S, Cruz H. A non-linear 3D FEM model to simulate timber–concrete joints. Adv Eng Softw 2007;38(8–9):522–30.

[50] Khorsandnia N, Valipour H, Crews K. Structural response of timber-concrete composite beams predicted by finite element models and manual calculations. Adv Struct Eng 2014;17(11):1601–21.

[51] Zona A, Barbato M, Fragiacomo M. Finite-element model updating and probabilistic analysis of timber-concrete composite beams. J Struct Eng 2011;138(7):899–910.

[52] Gelfi P, Giuriani E. Modello teorico del legame costitutivo per le connessioni a piolo. Studi E Ric Costr Cem Armato Frat Pasenti 1987;9:323–41.

[53] Fragiacomo M. A finite element model for long-term analysis of timber-concrete composite beams. Struct Eng Mech 2005;20(2):173–89.

[54] Möhler K. On the load carrying behavior of beams and columns of compound sections with flexible connections. Technical Univ. of Karlsruhe Germany; 1956.

[55] Renaudin F. Etude d'une poutre mixte bois - béton présentant une raideur de connexion finie. Cerema, Mar; 2016.

[56] Selçukoglu E, Zwicky D. Towards the plastic design of glulam concrete composite structures. IABSE Symp Rep 2009;96(4):20–9. https://doi.org/10.2749/222137809796088837.

[57] Auclair-Cuerrier S, Sorelli L, Salenikovich A. A new composite connector for timber-concrete composite structures. Constr Build Mater 2016;112:84–92.

[58] Gendron B, Salenikovich A, Sorelli L. Timber concrete composite beams with ductile connection. In: World Conference on Timber Engineering; 2016.

[59] Zhang C. Analysis of the timber-concrete composite systems with ductile connection. Canada: University of Toronto; 2013.

[60] ULaval. Guide d'utilisation DDuctile-TCS 1.0. Université Laval; 2017.

[61] Gauvreau P. Seismic analysis of concrete bridge piers: practical considerations in proceedings of the seventh canadian conference on earthquake engineering, Montreal, Canada; 1995.

[62] Lafarge. Product data sheet - Ductal JS1000; 2018.

[63] Matériaux King et Compagnie. King HP-S10 - Fiche technique; 2018.

[64] Gendron B. Ponts composites bois-béton en portée simple : théorie, essais et conception. Québec, Canada: Université Laval; 2016.

[65] CSA Group. CSA-A23.3-14 Calcul des ouvrages en béton. Canada; 2014.

[66] CSA Group. CSA S16-14 Design of steel structures. Canada; 2014.

[67] Nordic Structures. Design Properties Nordic Lam; Mar. 11, 2015.

[68] Schanack F, Ramos ÓR, Reyes JP, Low AA. Experimental study on the influence of concrete cracking on timber concrete composite beams. Eng Struct 2015;84:362–7.